PHYSICAL REVIEW D **94,** 034016 (2016)

From quarks and gluons to hadrons: Chiral symmetry breaking in dynamical QCD

Jens Braun,[1,2] Leonard Fister,[3] Jan M. Pawlowski,[4,2] and Fabian Rennecke[4,2]

[1]*Institut für Kernphysik (Theoriezentrum), Technische Universität Darmstadt, Schloß gartenstraß e 2, D-64289 Darmstadt, Germany*

[2]*ExtreMe Matter Institute EMMI, GSI, Planckstraße 1, D-64291 Darmstadt, Germany*

[3]*Institut de Physique Théorique, CEA Saclay, F-91191 Gif-sur-Yvette, France*

[4]*Institut für Theoretische Physik, Universität Heidelberg, Philosophenweg 16, 69120 Heidelberg, Germany*

(Received 13 January 2015; published 8 August 2016)

We present an analysis of the dynamics of two-flavor QCD in the vacuum. Special attention is paid to the transition from the high-energy quark-gluon regime to the low-energy regime governed by hadron dynamics. This is done within a functional renormalization group approach to QCD amended by dynamical hadronization techniques. These techniques allow us to describe conveniently the transition from the perturbative high-energy regime to the nonperturbative low-energy limit without suffering from a fine-tuning of model parameters. In the present work, we apply these techniques to two-flavor QCD with physical quark masses and show how the dynamics of the dominant low-energy degrees of freedom emerge from the underlying quark-gluon dynamics.

DOI: 10.1103/PhysRevD.94.034016

I. INTRODUCTION

For an accurate first-principles description of the dynamics of QCD, a reliable inclusion of hadronic states is of great importance. This holds in particular for an approach aiming at the hadron spectrum or the phase structure of QCD at finite density. In the present work on two-flavor QCD we develop a theoretical framework for taking into account the fluctuation dynamics of quarks, gluon and hadrons. This approach is based on previous functional renormalization group studies [1,2] and a related quantitative study in the quenched limit [3]. The present work and [3] are first works within a collaboration (fQCD) aiming at a quantitative functional renormalization group framework for QCD [4]. This framework allows us to dynamically include hadronic states as they emerge from the microscopic quark and gluon degrees of freedom.

We use the functional renormalization group (FRG) approach for QCD; for reviews see [5–14], and [15–21] for reviews on related work. In order to describe the transition from quarks and gluons to hadrons, we extend the dynamical hadronization technique (or rebosonization), introduced in Refs. [7,22–24]. For the first time, this technique is applied here to dynamical two-flavor QCD with physical quark masses. It is shown how the dominant hadronic low-energy degrees of freedom and their dynamics emerge from the underlying quark-gluon dynamics. The hadronization technique, as further developed in the present work, was already applied in Ref. [3] in a quantitative study of quenched QCD. In [3], a large number of interaction channels were taken into account, aimed at full quantitative precision. Here, we exploit the results from [3] as well as results on the scale-dependent glue sector of Yang-Mills theory from Refs. [18,25,26]. This enables us to concentrate on the RG flows of the most relevant couplings from a more phenomenological point of view, paying special attention to unquenching effects.

In summary, the aim of this work is threefold: firstly, we aim at a detailed understanding of the fluctuation physics in the transition region between the high-energy quark-gluon regime to the low-energy hadronic regime. Secondly, we want to initiate the quest for the minimal set of composite operators that has to be taken into account for reaching (semi)quantitative precision, while keeping the study analytic. This deepens the understanding of the fluctuation physics by only taking into account the relevant operators. Moreover, it is also of great interest for low-energy effective models. Thirdly, we discuss full unquenching effects in terms of the matter back-coupling to the glue sector that is important for QCD regimes with dominant quark fluctuations such as QCD at high densities or many flavors.

The paper is organized as follows: in Sec. II we introduce the ansatz for the quantum effective action which we are considering in the present work. The general framework of dynamical hadronization is then discussed in detail in Sec. III, where we also give a discussion of the RG flow in the gauge sector and the role of the quark-gluon vertex. Our results for two-flavor QCD are then presented in Sec. IV. While our analysis suggests that the use of dynamical hadronization techniques only yields mild quantitative corrections in low-energy model studies, its use is indispensable from both a qualitative and a quantitative point of view for a unified description of the

dynamics of QCD on all scales. Our conclusions are given in Sec. V. Some technical details as well as a brief discussion about the effect of dynamical hadronization on low-energy models are discussed in the appendixes.

II. THE EFFECTIVE ACTION

Our aim is to describe two-flavor QCD in $d = 4$ Euclidean dimensions at vanishing temperature and density in a vertex expansion. The starting point is the microscopic gauge-fixed QCD action. Thus, we include the quark-gluon, three- and four-gluon vertices as well as the ghost-gluon vertex and the corresponding momentum-dependent propagators. Four-quark interactions are dynamically generated at lower scales and we therefore take the scalar-pseudoscalar channel into account in our truncation. This is by far the dominant four-quark channel, as it exhibits quark condensation; see [3].

On even lower energy scales, bound state degrees of freedom appear and eventually become dynamical. To properly take this into account, we introduce a scale-dependent effective potential V_k which includes arbitrary orders of mesonic self-interactions. Since the dynamics in this sector is dominated by the lightest mesons, we restrict our analysis to pions and the sigma-meson and their corresponding momentum-dependent propagators. We therefore assume a strong axial anomaly; i.e. $U(1)_A$ is maximally broken. As a consequence, the meson sector in the chiral limit exhibits an $O(4)$ flavor symmetry. Note that this is also reflected in the four-quark interaction: the scalar-pseudoscalar channel $\sim\lambda_{q,k}$ is invariant under $SU(2)_V \times SU(2)_A$ but violates $U(1)_A$ symmetry; see (1). Explicit chiral symmetry breaking is included via a source term $-c\sigma$. It is directly related to a finite current quark mass and, as a consequence, nonzero pion masses. This implies that we have a chiral crossover transition rather than a second order phase transition. The meson sector is coupled to the quark sector by a field-dependent Yukawa coupling $h_k(\phi^2)$. That way, arbitrarily high orders of quark-antiquark multimeson correlators are included [27]. We elaborate on the physics picture in Sec. IV.

The key mechanism to consistently describe the dynamical generation of bound state degrees of freedom in this work is dynamical hadronization, and is discussed in Sec. III A. In summary, this yields the following scale-dependent effective action,

$$\begin{aligned}\Gamma_k = \int_x \Big\{ & \frac{1}{4} F^a_{\mu\nu} F^a_{\mu\nu} + Z_{c,k} \bar{c}^a \partial_\mu D^{ab}_\mu c^b + \frac{1}{2\xi} (\partial_\mu A^a_\mu)^2 \\ & + Z_{q,k} \bar{q} (\gamma_\mu D_\mu) q - \lambda_{q,k} [(\bar{q} T^0 q)^2 - (\bar{q} \gamma_5 \vec{T} q)^2] \\ & + h_k(\phi^2) [\bar{q} (i\gamma_5 \vec{T}\,\vec{\pi} + T^0 \sigma) q] + \frac{1}{2} Z_{\phi,k} (\partial_\mu \phi)^2 \\ & + V_k(\rho) - c\sigma \Big\} + \Delta\Gamma_{\text{glue}}, \end{aligned} \tag{1}$$

with the $O(4)$ meson field $\phi = (\sigma, \vec{\pi})$ and $\rho = \phi^2/2$. $D_\mu = \partial_\mu - i Z^{1/2}_{A,k} g_k A^a_\mu t^a$ is the Dirac operator, with the strong coupling $g_k = \sqrt{4\pi\alpha_{s,k}}$ and the gluonic wave-function renormalization $Z_{A,k}$. With this definition the covariant derivative D_μ is renormalization group invariant. The last term in the first line, $\Delta\Gamma_{\text{glue}}$, stands for the nontrivial ghost-gluon, three-gluon and four-gluon vertex corrections; for further details see Sec. III C and in particular Eq. (70). The full momentum dependence of the pure gauge sector is taken into account in the gluon and ghost dressing functions $Z_{A,k}$ and $Z_{c,k}$. This is crucial for the correct IR behavior of the gauge sector.

Due to asymptotic freedom the effective action at the initial cutoff scale Λ relates to the classical (gauge-fixed) QCD action,

$$\begin{aligned}\Gamma_{k\to\Lambda} \simeq \int_x \Big\{ & \frac{1}{4} F^a_{\mu\nu} F^a_{\mu\nu} + \bar{q} (\gamma_\mu D_\mu + m_q^{\text{UV}}) q \\ & + \bar{c}^a \partial_\mu D^{ab}_\mu c^b + \frac{1}{2\xi} (\partial_\mu A^a_\mu)^2 \Big\}. \end{aligned} \tag{2}$$

The quark mass m_q^{UV} at the UV scale Λ is directly related to the coupling c in Eq. (1). The other couplings appearing in our ansatz (1) for the effective action are generated dynamically in the RG flow.

In this work, we use Hermitian gamma matrices so that

$$\{\gamma_\mu, \gamma_\nu\} = 2\delta_{\mu\nu} \mathbb{1}. \tag{3}$$

The commutator for the $SU(N_c)$ generators reads $[t^a, t^b] = i f^{abc} t^c$ and, hence, the trace is positive, $\text{Tr} t^a t^b = \frac{1}{2}\delta^{ab}$. $\vec{T}$ are the $SU(N_f)$ generators and $T^0 = \frac{1}{\sqrt{2N_f}} \mathbb{1}_{N_f \times N_f}$. For the field strength tensor we use the relation

$$\begin{aligned} F_{\mu\nu} &= \frac{i}{Z^{1/2}_{A,k} g_k} [D_\mu, D_\nu] \\ &= Z^{1/2}_{A,k} t^a (\partial_\mu A^a_\nu - \partial_\nu A^a_\mu + Z^{1/2}_{A,k} g_k f^{abc} A^b_\mu A^c_\nu). \end{aligned} \tag{4}$$

For more details on the gauge part of our truncation see Sec. III C. All masses, wave-function renormalizations and couplings are scale dependent. The scalar potential and the Yukawa coupling are expanded about a scale-independent point κ, $\partial_t \kappa = 0$. As shown in [27] this yields a rapid convergence of the expansion

$$\begin{aligned} V_k(\rho) &= \sum_{n=1}^{N_V} \frac{v_{n,k}}{n!} (\rho - \kappa)^n, \\ h_k(\rho) &= \sum_{n=0}^{N_h} \frac{h_{n,k}}{n!} (\rho - \kappa)^n. \end{aligned} \tag{5}$$

Note that the quark and meson mass functions (two-point functions at vanishing momentum) depend on the meson

fields. The masses are given by the mass functions evaluated at the physical minimum $\rho_{0,k} = \sigma_0^2/2$ of $V_k(\rho) - c\sigma$,

$$\begin{aligned} m_{q,k}^2 &= \frac{1}{2} h_k^2(\rho_{0,k})\rho_{0,k}, \\ m_{\pi,k}^2 &= V'(\rho_{0,k}), \\ m_{\sigma,k}^2 &= V'(\rho_{0,k}) + 2\rho_{0,k}V''(\rho_{0,k}), \end{aligned} \tag{6}$$

where $m_{q,k}$ is the constituent quark mass. The current quark mass m_q^{UV} is related to the symmetry breaking source c via the mass function at the ultraviolet scale,

$$m_q^{\mathrm{UV}} = \frac{h_\Lambda}{2v_{1,\Lambda}} c, \tag{7}$$

while c does not occur explicitly in the flow equation as it is the coefficient of a one-point function. This entails that the flows of the effective action in the chiral limit and that in QCD with nonvanishing current quark masses agree; see also [27]. The difference solely relates to the solution of the equation of motion for the σ-field,

$$\left.\frac{\delta\Gamma_{k=0}}{\delta\sigma}\right|_{\sigma=\sigma_{\mathrm{EoM}}} = 0. \tag{8}$$

If expanding the flow in powers of the mesonic fields as done in the present work, the expansion point has to be close to σ_{EoM}, such that it is within the radius of convergence of the expansion.

III. QUANTUM FLUCTUATIONS

Quantum fluctuations are computed with the functional renormalization group. For QCD related reviews and corresponding low-energy models, we refer the reader to Refs. [5–14]. A consistent description of the dynamical transition from quark-gluon degrees of freedom to hadronic degrees of freedom is achieved by the dynamical hadronization technique. Loosely speaking, it is a way of storing four-quark interaction channels, which are resonant at the chiral phase transition, in mesonic degrees of freedom and therefore allows for a unified description of the different degrees of freedom governing the dynamics at different momentum scales.

A. Functional RG and dynamical hadronization

The starting point of the functional renormalization group is the scale-dependent effective action Γ_Λ at a UV-cutoff scale Λ. In the case of QCD, Λ is a large, perturbative energy scale and correspondingly Γ_Λ is the microscopic QCD action with the strong coupling constant and the current quark masses as the only free parameters of the theory. From there, quantum fluctuations are successively included by integrating out momentum shells down to the RG scale k. This yields the scale-dependent effective action Γ_k, which includes all fluctuations from momentum modes with momenta larger than k. By lowering k we resolve the macroscopic properties of the system and eventually arrive at the full quantum effective action $\Gamma = \Gamma_{k=0}$. The RG evolution of the scale-dependent effective action is given by the Wetterich equation [28], which in the case of QCD with $\Phi = (A, q, \bar{q}, c, \bar{c}, \phi)$ reads

$$\begin{aligned} \partial_t\Gamma_k[\Phi] = &\frac{1}{2}\mathrm{Tr}(G_{AA,k}[\Phi]\partial_t R_k^A) - \mathrm{Tr}(G_{c\bar{c},k}[\Phi]\partial_t R_k^c) \\ &- \mathrm{Tr}(G_{q\bar{q},k}[\Phi]\partial_t R_k^q) + \frac{1}{2}\mathrm{Tr}(G_{\phi\phi,k}[\Phi]\partial_t R_k^\phi). \end{aligned} \tag{9}$$

Here, the regulator functions $R_k^{\Phi_i}(p)$ can be understood as momentum-dependent masses that introduce the suppression of infrared modes of the respective field Φ_i, and are detailed in Appendix C. The derivative ∂_t is the total derivative with respect to the RG scale $t = \ln(k/\Lambda)$ with some reference scale Λ. The traces sum over discrete and continuous indices of the fields, including momenta and species of fields. The first line on the right-hand side of (9) is the flow in the pure glue sector; the second line creates the matter fluctuations. $G_k[\Phi]$ denote the scale and field-dependent full propagators of the respective fields, e.g. for the quarks:

$$G_{q\bar{q},k}[\Phi] = \left(\frac{\delta^2\Gamma_k[\Phi]}{\delta q(-p)\delta\bar{q}(p)} + R_k^q\right)^{-1}. \tag{10}$$

In the following, we will not encounter mixed two-point functions. Hence, it is sufficient to define these expressions for the combinations quark-antiquark, meson-meson, gluon-gluon (both transverse) and ghost-antighost. For the rest of the manuscript, we drop the redundant second field index for the two-point functions and the propagators. In a slight abuse of notation we define the scalar parts of the two-point functions of the quark, meson, gluon and ghost as

$$\begin{aligned} \Gamma_{q,k}^{(2)}(p) &\equiv \frac{\delta^2\Gamma_k[\Phi]}{\delta q(-p)\delta\bar{q}(p)}, & \Gamma_{\phi,k}^{(2)}(p) &\equiv \frac{\delta^2\Gamma_k[\Phi]}{\delta\phi(-p)\delta\phi(p)}, \\ \Gamma_{A,k}^{(2)}(p) &\equiv \frac{\delta^2\Gamma_k[\Phi]}{\delta A(-p)\delta A(p)}, & \Gamma_{c,k}^{(2)}(p) &\equiv \frac{\delta^2\Gamma_k[\Phi]}{\delta c(-p)\delta\bar{c}(p)}. \end{aligned} \tag{11}$$

With this we define the corresponding wave-function renormalizations and (scalar parts of the) propagators

$$\begin{aligned} Z_{\Phi_i,k}(p) &= \Delta\Gamma_{\Phi_i,k}^{(2)}(p)/\Delta S_{\Phi_i}^{(2)}(p)|_{\text{scalar part}}, \\ G_{\Phi_i,k}(p) &= \left(Z_{\Phi_i,k}(p)\Delta S_{\Phi_i}^{(2)} + R_k^{\Phi_i}(p)\right)^{-1}|_{\text{scalar part}}, \end{aligned} \tag{12}$$

with $\Phi_i = q, \phi, A$ or c. The scalar part is the coefficient of the tensor structure of the expressions above. In (12) we have $\Delta\Gamma^{(2)}_{\Phi_i,k}(p) = \Gamma^{(2)}_{\Phi_i,k}(p) - \Gamma^{(2)}_{\Phi_i,k}(0)$ for all fields except for the gluon, where $\Delta\Gamma^{(2)}_{A,k}(p) = \Gamma^{(2)}_{A,k}(p)$. The same holds true for $\Delta S^{(2)}_{\Phi_i}$. At $k = 0$ and the fields set to their vacuum expectation value, $G_{\Phi_i,k=0}(p)$ is the full propagator. The above definitions are exemplified with the full gluon propagator,

$$G^{ab}_{A,k}(p) = \frac{1}{Z_{A,k}(p)p^2 + R^A_k}\Pi^{\perp}\delta^{ab}, \tag{13}$$

with the transversal projection operator $\Pi^{\perp}$; see (C2). For our calculations, we use four-dimensional Litim regulators R_k [29]; for details see Appendix C.

In the infrared regime of QCD, the dynamical degrees of freedom are hadrons, while quarks and gluons are confined inside hadrons. This entails that a formulation in terms of local composite fields with hadronic quantum numbers is more efficient in this regime. Note that these composite fields are directly related to hadronic observables at their poles.

Let us illustrate this at the relevant example of the scalar-pseudoscalar mesonic multiplet at a given cutoff scale k. At a fixed large cutoff scale, where the mesonic potential $V_k(\rho)$ is assumed to be Gaussian, we can resort to the conventional Hubbard-Stratonovich bosonization: the local part of the scalar-pseudoscalar channel of the four-quark interaction with coupling $\lambda_{q,k}$ [see the second line in (1)] can be rewritten as a quark-meson term [see the third line in (1)] on the equations of motion for ϕ, that is ϕ_{EoM}. This leads to

$$\lambda_{q,k} = \frac{h_k^2}{2v_{1,k}}, \qquad \phi_{j,\mathrm{EoM}} = \frac{h_k}{v_{1,k}}\bar{q}\boldsymbol{\tau}_j q, \tag{14}$$

where v_1 is the curvature mass of the mesonic field and $\boldsymbol{\tau} = (\gamma_5\vec{T}, iT^0)$, $j \in \{1,2,3,4\}$. Note that (14) is only valid for $Z_\phi \equiv 0$ and a Gaussian potential $V_k(\rho) = v_1\rho$. Moreover, miscounting of degrees of freedom may occur from an inconsistent distribution of the original four-fermi interaction strength to the Yukawa coupling and the four-fermi coupling. The dynamical hadronization technique used in the present work, and explained below, resolves these potential problems.

One advantage of the bosonized formulation concerns the direct access to spontaneous chiral symmetry breaking via the order parameter potential $V_k(\rho)$: spontaneous symmetry breaking is signaled by $v_1 = 0$ at the symmetry breaking scale k_χ which relates to a resonant four-quark interaction. It also facilitates the access to the symmetry-broken infrared regime.

Let us now assume that we have performed the above complete bosonization at some momentum scale $k \gg k_\chi$.

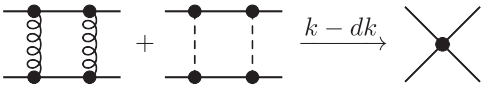

FIG. 1. Regeneration of four-quark interactions from the RG flow.

There, the above conditions for the bosonization in (14) are valid. Hence, we can remove the four-fermi term completely in favor of the mesonic Yukawa sector. However, four-quark interactions are dynamically regenerated from the RG flow via quark-gluon and quark-meson interactions; see Fig. 1.

Indeed, these dynamically generated contributions dominate due to the increase of the strong coupling $\alpha_{s,k}$ for a large momentum regime, leading to a quasifixed point running of the Yukawa coupling; see Refs. [3,22,23] and Sec. IV. Thus, even though $\lambda_{q,k}$ was exactly replaced by $m_{\phi,k}$ and h_k at a scale $k \gg k_\chi$, there is still a nonvanishing RG flow of $\lambda_{q,k}$ at lower scales. Note, however, that we have explicitly checked that this is only a minor quantitative effect as long as one considers low-energy effective models; see Appendix A.

In summary, it is not possible to capture the full dynamics of the system in the quark-gluon regime with the conventional Hubbard-Stratonovich bosonization. As a consequence, with the conventional bosonization, the scale where composite fields take over the dynamics from fundamental quarks and gluons is not an emergent scale generated by the dynamics of QCD, but is fixed by hand by the scale where the Hubbard-Stratonovich transformation is performed.

In the present approach we employ dynamical hadronization instead of the conventional bosonization. It is a formal tool that allows for a unified description of dynamically changing degrees of freedom and consequently is not plagued by the shortcomings of conventional bosonization discussed above. It has been introduced in [22] and was further developed in [7,23,24]. The construction works for general potentials $V_k(\rho)$ (more precisely general $\Gamma_k[\Phi]$), and implements the idea of bosonizing multifermion interactions at every scale k rather just at the initial scale. Consequently, the resulting fields of this bosonization procedure, i.e. the mesons, become scale dependent and can be viewed as hybrid fields: while they act as conventional mesons at low energies, they encode pure quark dynamics at large energy scales.

Here we follow the dynamical hadronization setup put forward in [7] and outline the derivation of the flow equation in the presence of scale-dependent meson fields. The starting point is the functional integral representation of the scale-dependent effective action Γ_k with scale-dependent meson fields. To this end, we define the dynamical superfield $\hat{\Phi}_k = (\hat{\varphi}, \hat{\phi}_k)$, where the microscopic fields are combined in $\hat{\varphi} = (\hat{A}_\mu, \hat{q}, \hat{\bar{q}}, \hat{c}, \hat{\bar{c}})$ and the scale-dependent meson fields, in our case pions and the sigma

meson, are represented by the $O(4)$ field $\hat{\phi}_k = (\hat{\vec{\pi}}_k, \hat{\sigma}_k)$. The path integral representation of Γ_k reads

$$e^{-\Gamma_k[\Phi_k]} = \int \mathcal{D}\hat{\varphi} \exp\Big\{-S[\hat{\varphi}] - \Delta S_k[\hat{\Phi}_k] + \frac{\delta(\Gamma_k + \Delta S_k)}{\delta \Phi_k}(\hat{\Phi}_k - \Phi_k) + \Delta S_k[\Phi_k]\Big\}, \quad (15)$$

where we defined the expectation value of the fields $\Phi_k = \langle \hat{\Phi}_k \rangle$ and used

$$J = \frac{\delta(\Gamma_k + \Delta S_k)}{\delta \Phi_k} \quad \text{and} \quad \Delta S_k[\Phi_k] = \frac{1}{2}\Phi_k R_k \Phi_k. \quad (16)$$

Note that the functional integral in (15) contains only the fundamental fields $\hat{\varphi}$ of QCD. Composite operators such as the (scale-dependent) mesons are introduced via corresponding source terms in the Schwinger functional; see [7].

To arrive at the evolution equation for $\Gamma_k[\Phi_k]$, we take the scale derivative $\partial_t = k\frac{d}{dk}$ of Eq. (15). The RG evolution of the scale-dependent composite meson fields is of the form

$$\partial_t \hat{\phi}_k = \dot{A}_k \bar{q}\boldsymbol{\tau} q + \dot{B}_k \hat{\phi}_k. \quad (17)$$

The first part of this equations reflects the bound state nature of the mesons. The second part corresponds to a general rescaling of the fields. The coefficients $\dot{A}_k$ and $\dot{B}_k$, which we call hadronization functions, are specified below. Note that the right-hand side of (17) only involves the quark mean fields $q = \langle \hat{q} \rangle$, $\bar{q} = \langle \hat{\bar{q}} \rangle$. An explicit solution to this equation is given by

$$\hat{\phi}_k = C_k e^{B_k} \bar{q}\boldsymbol{\tau} q, \quad (18)$$

with $\dot{A}_k = \dot{C}_k e^{B_k}$. This reflects the quark-antiquark nature of the meson. Equation (17) leads to the following identity for the flow of the hadronization field,

$$\langle \partial_t \hat{\phi}_k \rangle = \dot{A}_k \bar{q}\boldsymbol{\tau} q + \dot{B}_k \phi_k, \quad (19)$$

and furthermore $\langle \partial_t \hat{\phi}_k \rangle = \partial_t \phi_k$. Taking (17) into account, the scale derivative of (15) gives a modified version of the flow equation (9). While the gauge and quark parts of the equation remain unchanged, the mesonic part now reads

$$\partial_t|_\phi \Gamma_k[\Phi_k] = \frac{1}{2}\mathrm{Tr}[G_{\phi\phi,k}[\Phi] \cdot (\partial_t R_k^\phi + 2R_k^\phi \dot{B}_k)] - \mathrm{Tr}\left[\frac{\delta \Gamma_k[\Phi]}{\delta \phi_i}(\dot{A}_k \bar{q}\boldsymbol{\tau_i} q + \dot{B}_k \phi_i)\right]. \quad (20)$$

The first line of (20) corresponds to the mesonic part of the flow equation (9) with a shift in the scale derivative of the regulator owing to the part of $\partial_t \phi_k$ which is proportional to ϕ_k itself. Note that (20) remains valid for the more general flow of the superfield [7]

$$\partial_t \hat{\Phi}_{i,k} = \dot{A}_{ij,k} \cdot F_{j,k}[\Phi_k] + \dot{B}_{ij,k}[\Phi_k]\hat{\Phi}_{j,k}, \quad (21)$$

where $F[\Phi_k]$ is any functional of the mean superfield Φ_k. We emphasize that the 1-loop nature of the flow equation is not spoiled as long as $\partial_t \hat{\Phi}_{i,k}$ is at most linear in the quantum field $\hat{\Phi}_{i,k}$. It can, in fact, be an arbitrary function of the mean fields $\Phi_{i,k}$ without altering the properties of the flow equation. The meson regulator has the form (see Appendix C)

$$R_k^\phi(p^2) = Z_{\phi,k} p^2 r_B(p^2/k^2), \quad (22)$$

and its corresponding scale derivative can conveniently be written as

$$\partial_t R_k^\phi(p^2) = (\partial_t|_Z - \eta_{\phi,k}) R_k^\phi(p^2), \quad (23)$$

with the anomalous dimension of the scale-dependent mesons,

$$\eta_{\phi,k} = -\frac{\partial_t Z_{\phi,k}}{Z_{\phi,k}}. \quad (24)$$

This choice of the regulator functions implies that the flow equations of RG-invariant quantities only contain the anomalous dimension which stems from the scale derivative of the regulator whereas the wave-function renormalizations drop out completely. With this, we can rewrite (20) into

$$\partial_t|_\phi \Gamma_k[\Phi_k] = \frac{1}{2}\mathrm{Tr}[G_{\phi\phi,k}[\Phi] \cdot (\partial_t|_Z - (\eta_{\phi,k} - 2\dot{B}_k))R_k^\phi] - \mathrm{Tr}\left[\frac{\delta \Gamma_k[\Phi]}{\delta \phi_i}(\dot{A}_k \bar{q}\boldsymbol{\tau_i} q + \dot{B}_k \phi_i)\right]. \quad (25)$$

It is now obvious that the first line of the modified flow equation above gives the original flow equations without scale-dependent fields, but with a shifted meson anomalous dimension:

$$\eta_{\phi,k} \to \eta_{\phi,k} - 2\dot{B}_k. \quad (26)$$

The other coefficient, $\dot{B}_k$, in (17) is at our disposal, and we may use it to improve our truncation.

The second line of (20) induces additional contributions in particular to the flows of the four-quark and the Yukawa coupling, owing to the particular ansatz we made for $\partial_t \phi_k$. This allows us to specify the hadronization procedure: we choose the coefficient $\dot{A}_k$ such that the flow of the four-quark interaction $\lambda_{q,k}$ vanishes within our truncation, $\partial_t \lambda_{q,k} = 0$. This way, all information about the multiquark

correlations are stored in the flow of the Yukawa coupling. Thus, h_k encodes the multiquark correlations in the quark-gluon regime and the meson-constituent-quark correlations in the hadronic regime, including a dynamical transition between these different regimes.

B. Hadronized flow equations

In the following we specify the hadronization procedure and give the resulting modified flow equations of the scale-dependent parameters of the truncation (1). These modifications are given by explicitly evaluating the second line of (20). Note that the explicit form of the modified flow equations depends on the details of our projection procedures; see also Appendix B.

In the following, we rescale all fields with their respective wave-function renormalization, $\bar{\Phi} = \sqrt{Z_{\Phi,k}}\Phi$, and introduce the RG-invariant parameters

$$\bar{g}_k = \frac{g_k}{Z_{q,k}Z_{A,k}^{1/2}}, \qquad \bar{\lambda}_{q,k} = \frac{\lambda_{q,k}}{Z_{q,k}^2}, \qquad \bar{c}_k = \frac{c}{Z_{\phi,k}},$$
$$\bar{\lambda}_{n,k} = \frac{\lambda_{n,k}}{Z_{\phi,k}^n}, \quad \bar{h}_{n,k} = \frac{h_{n,k}}{Z_{q,k}Z_{\phi,k}^{(2n+1)/2}}, \quad \bar{\kappa}_k = Z_{\phi,k}\kappa. \tag{27}$$

Note that the parameters defined in (27) do scale with the infrared cutoff scale k, but are invariant under general RG transformations (reparametrizations) of QCD. For example, $\bar{g}_k$ is nothing but the running strong coupling. The RG-invariant dimensionless masses are defined accordingly as

$$\bar{m}_{q,k} = \frac{m_{q,k}}{kZ_{q,k}} \quad \text{and} \quad \bar{m}_{\pi/\sigma,k} = \frac{m_{\pi/\sigma,k}}{kZ_{\phi,k}^{1/2}}. \tag{28}$$

Note that we rescale mesonic parameters with the wave-function renormalization $Z_{\phi,k}$ of the scale-dependent mesons ϕ_k. The constant source c as well as the expansion point κ have only canonical running after rescaling, given only by the running of $Z_{\phi,k}$; see Eq. (B3). Consequently, we also rescale the hadronization functions and, in addition, define them to be dimensionless:

$$\dot{\bar{A}}_k = k^2 Z_{\phi,k}^{1/2} Z_{q,k}^{-1} \dot{A}_k, \qquad \dot{\bar{B}}_k = \dot{B}_k. \tag{29}$$

With this, we proceed now to the modified flow equations of these RG-invariant quantities.

For the flow of the four-quark interaction $\bar{\lambda}_{q,k}$ we find

$$\partial_t|_\phi \bar{\lambda}_{q,k} = 2\eta_{q,k}\bar{\lambda}_{q,k} + \partial_t \bar{\lambda}_{q,k}|_{\eta_{\phi,k}\to\tilde{\eta}_{\phi,k}-2\dot{\bar{B}}_k} + \left(\bar{h}_k(\bar{\rho}) + 2\bar{\rho}\bar{h}_k'(\bar{\rho})\frac{4N_fN_c-1}{2N_fN_c+1}\right)\dot{\bar{A}}_k. \tag{30}$$

Here, $\partial_t \bar{\lambda}_{q,k}$ denotes the flow without dynamical hadronization which is specified in Appendix B. As already discussed above, this contribution is subject to a shift in the meson anomalous dimension, indicated by $\eta_{\phi,k} \to \eta_{\phi,k} - 2\dot{\bar{B}}_k$.

Following the discussion in the previous section, we choose $\dot{\bar{A}}_k$ such that the flow of $\bar{\lambda}_{q,k}$ vanishes. This is achieved by the following choice:

$$\dot{\bar{A}}_k = -\left(\bar{h}_k(\bar{\rho}) + 2\bar{\rho}\bar{h}_k'(\bar{\rho})\frac{4N_fN_c-1}{2N_fN_c+1}\right)^{-1} \times \partial_t \bar{\lambda}_{q,k}|_{\eta_{\phi,k}\to\eta_{\phi,k}-2\dot{\bar{B}}_k}. \tag{31}$$

Together with the initial condition $\bar{\lambda}_{q,\Lambda} = 0$, this yields

$$\partial_t|_\phi \bar{\lambda}_{q,k} = 0. \tag{32}$$

The flow of the Yukawa coupling assumes the following form:

$$\partial_t|_\phi \bar{h}_k = \left(\eta_{q,k} + \frac{1}{2}\eta_{\phi,k}\right)\bar{h}_k + \partial_t \bar{h}_k|_{\eta_{\phi,k}\to\tilde{\eta}_{\phi,k}-2\dot{\bar{B}}_k} - \frac{1}{k^2}(p^2 + \bar{V}_k'(\bar{\rho}))\dot{\bar{A}}_k - (\bar{h}_k + 2\bar{\rho}\bar{h}_k')\dot{\bar{B}}_k, \tag{33}$$

where $\bar{h}_k = \bar{h}_k(\bar{\rho})$ is implied and $\partial_t \bar{h}_k$ is specified in Appendix B. From Eq. (31), it is now clear that the flow of the quark interaction and, therefore, all information about the multiquark correlations within our truncation is incorporated into the flow of the hadronized Yukawa coupling.

It is left to specify the hadronization function $\dot{\bar{B}}_k$, which also enters (33). We see from Eq. (18) that it corresponds to a phase factor of the hadronization field. It can be used to improve the current approximation by absorbing a part of the momentum dependence of the mesonic wave-function renormalization and the Yukawa coupling. This will be discussed elsewhere. Here, we use

$$\dot{B}_k \equiv 0, \tag{34}$$

for the sake of simplicity. We see that our hadronization procedure enforces a vanishing four-quark interaction. The effect of four-quark correlations is then stored in the Yukawa coupling, which now serves a dual purpose: while it captures the current-quark self-interactions in the quark-gluon regime, it describes the meson-constituent-quark in the hadronic regime.

C. Gauge sector

In this section, we discuss the gauge sector of the truncation given in (1). Most importantly, this permits us to distinguish the quark-gluon coupling from pure gluodynamics. This directly signals the transition from the perturbative quark-gluon regime at large momenta, where

all couplings scale canonically, to the hadronic regime where nonperturbative effects are dominant.

The couplings induced from three-point functions play a dominant role in the description of interactions. Hence, we solve the flow equations for all three-point functions in QCD, the quark-gluon, three-gluon and ghost-gluon vertices. In addition, the effects from the four-gluon vertex are important [18,25,26]. Thus, we employ an ansatz which has proven to be accurate in previous studies [25,26]. For the computation presented here, we take the gluon and ghost propagators from pure gauge theory as input [18,25,26] and augment them by unquenching effects. In the perturbative domain this procedure is accurate, as the error is order $\alpha_{s,k}^2$. At scales below the confinement transition the gluon is gapped and therefore decouples from the dynamics.

Perturbation theory gives a direct relation between the number of gluon legs m attached to the vertex $\Gamma^{(n)}$ and the order in the strong coupling, $\Gamma^{(n)} \sim (4\pi\alpha_{s,k})^{m/2}$. Nevertheless, the RG running is different, although purely induced by the external legs attached. Their wave-function renormalizations cancel exactly those from the propagators; see (38) below. As a result of this truncation, the flow equations for couplings depend on the anomalous dimensions only.

In this analysis we restrict ourselves to classical tensor structures of the gauge action $S[\Phi]$. Omitting color and Lorentz indices for clarity, we parametrize the quark-gluon, three- and four-gluon and the ghost-gluon vertices as

$$\begin{aligned}
\Gamma_k^{(\bar{q}Aq)} &= Z_{A,k}^{\frac{1}{2}} Z_{q,k} g_{\bar{q}Aq,k} S_{\bar{q}Aq}^{(3)}, \\
\Gamma_k^{(A^3)} &= Z_{A,k}^{\frac{3}{2}} g_{A^3,k} S_{A^3}^{(3)}, \\
\Gamma_k^{(A^4)} &= Z_{A,k}^{2} g_{A^4,k}^2 S_{A^4}^{(4)}, \\
\Gamma_k^{(\bar{c}Ac)} &= Z_{A,k}^{\frac{1}{2}} Z_{c,k} g_{\bar{c}Ac,k} S_{\bar{c}Ac}^{(3)}.
\end{aligned} \tag{35}$$

The classical tensor structures $S^{(n)}_{\Phi_1\ldots\Phi_n}$ are obtained from (2) by

$$S^{(n)}_{\Phi_1\ldots\Phi_n} = \left.\frac{\delta^n \Gamma_\Lambda}{\delta\Phi_1\ldots\delta\Phi_n}\right|_{g_k=1}, \tag{36}$$

where we have omitted indices for clarity. In this work, we use as input the gluon/ghost two-point functions $\Gamma^{(2),\mathrm{YM}}_{A/c,k}(p)$ computed in [18,25,26] for pure Yang-Mills theory,

$$\begin{aligned}
\Gamma^{(2),\mathrm{YM}}_{A,k} &= Z^{\mathrm{YM}}_{A,k}(p) p^2 \Pi^{\perp}, \\
\Gamma^{(2),\mathrm{YM}}_{c,k} &= Z^{\mathrm{YM}}_{c,k}(p) p^2,
\end{aligned} \tag{37}$$

where the identity matrix in adjoint color space is implied. In Figs. 2 and 3 we show this input as a function of the momentum p for various k. Note that we show the regulated gluon propagator and ghost dressing function with optimized regulators $R_k^{A/c} = (Z^{\mathrm{YM}}_{A/c,k}(k)k^2 - Z^{\mathrm{YM}}_{A/c,k}(p)p^2)\theta(k^2 - p^2)$.

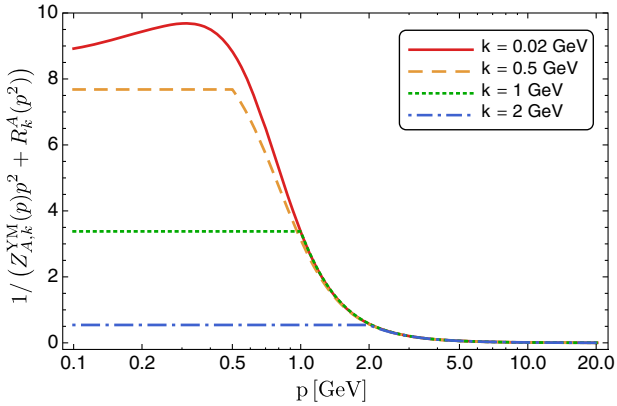

FIG. 2. The regulated gluon propagator from pure Yang-Mills theory as a function of the momentum for various k. We use this as an external input for our QCD computations.

We want to emphasize that a particular strength of the approach presented here is that it is independent of the specific form of the input in the sense that Yang-Mills propagators from any given method can be used. We have explicitly checked that our results are not altered if we use e.g. lattice input. In this case, the input dressing functions are of the form $Z^{\mathrm{YM}}_{A/c}(p) = Z^{\mathrm{YM}}_{A/c,k=0}(p)$ and the RG-scale dependence can be introduced by the identification $p = k$.

In order to make full use of the nontrivial input we use here, we expand the flow equation for the gluon propagator in QCD about that in Yang-Mills theory. We use the freedom in defining the cutoff function R_k^A to simplify the analysis. This is done by choosing the same prefactor $Z_{A,k}$ for the gluon regulator as for the vertex parametrizations in (35); see Eq. (C1). Note that the gluon propagator enters in loop integrals with momenta

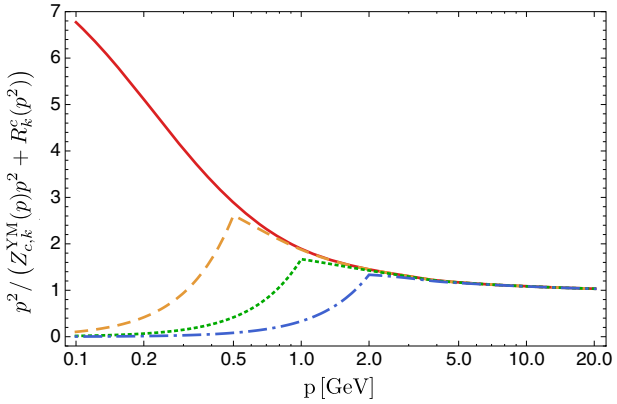

FIG. 3. The regulated ghost dressing function from pure Yang-Mills theory as a function of the momentum for various k. We use this as an external input for our QCD computations. The labeling is the same as in Fig. 2.

$p^2 \lesssim k^2$. If we estimate the full gluon propagator (13) with the simple expression (with the tensor structure omitted for clarity)

$$G_{A,k}(p) \approx \frac{1}{Z_{A,k}p^2 + R_k^A} = \frac{1}{Z_{A,k}} \frac{1}{p^2(1 + r_B(p^2/k^2))} \tag{38}$$

[i.e. we only consider the fully p-dependent $Z_{A,k}(p)$ evaluated at $p = k$], the system of flow equations considered is tremendously simplified. The error of such a simple estimate relates to

$$p^3 \left(\frac{1}{Z_{A,k}(p)p^2 + R_k^A} - \frac{1}{Z_{A,k}p^2 + R_k^A} \right)^n = p^{3+2n} \left(\frac{Z_{A,k} - Z_{A,k}(p)}{(Z_{A,k}(p)p^2 + R_k^A)(Z_{A,k}p^2 + R_k^A)} \right)^n, \tag{39}$$

where the factor p^3 stems from the momentum integration $\sim dp\, p^3$. The expression in (39) occurs with powers $n \geq 1$ in the difference of the full flow equations and the approximated flows with (38), and is evaluated for momenta $p^2 \lesssim k^2$. For small momenta it tends towards zero while its value for maximal momenta $p^2 \approx k^2$ is proportional to the difference $Z_{A,k} - Z_{A,k}(k)$. Consequently, we choose

$$Z_{A,k} = Z_{A,k}(k). \tag{40}$$

We have checked that the difference between full flows and approximated flows is less than 5% for all k.

Within approximations (35) and (38), the gluon propagator enters flow equations only via the anomalous dimension $\eta_{A,k}$ with

$$\eta_{A,k} = -\frac{\partial_t Z_{A,k}}{Z_{A,k}}. \tag{41}$$

As a consequence of (40), $\eta_{A,k}$ has two contributions from the full dressing function $Z_{A,k}(p)$,

$$\partial_t Z_{A,k} = \partial_t Z_{A,k}(p)|_{p^2=k^2} + k \frac{\partial Z_{A,k}(p)}{\partial p}\bigg|_{p^2=k^2}. \tag{42}$$

The first term stems from the genuine k-dependence of the dressing function, while the second term results from its momentum dependence. As is the case for any flow of a coupling in a gapped theory (away from potential fixed points), the first term of (42) vanishes in the limit $k \to 0$,

$$\lim_{k\to 0} \partial_t Z_{A,k}(p)|_{p^2=k^2} = 0. \tag{43}$$

The second term of (42) carries the information about the momentum dependence of the dressing function and in particular of the (bare) mass gap $m_{\rm gap}$ at small momenta. The gluon propagator exhibits a gap at small momentum scales and hence the dressing function of the full quantum theory, $Z_{A,k=0}(p)$, is of the form

$$\lim_{p^2\to 0} Z_{A,k=0}(p) \propto \frac{m_{\rm gap}^2}{p^2}. \tag{44}$$

This implies for the second term in (42)

$$\lim_{k\to 0} k\partial_p \ln (Z_{A,k}(p))|_{p^2=k^2} = -2. \tag{45}$$

Thus, the second term of (42) generates a nonvanishing gluon anomalous dimension $\eta_{A,k}$, as defined in (41) for $k \to 0$.

We note that this difference between the pure k-dependence and the momentum dependence of the gluon dressing function is both highly nontrivial and indispensable in any satisfactory truncation, even on a qualitative level. The RG-scale dependence alone does not suffice to capture the nonperturbative physics of YM theory or QCD in the gauge sector, as it misses the confining properties of the theory. Being of primary importance, the gluon mass gap emerges from the nontrivial momentum dependence of the propagator. We remark that this is in contrast to the chiral properties of the matter sector of QCD, where approximations based on solely k-dependent parameters at least qualitatively capture all the relevant physics.

It is crucial that $Z_{A,k}$ does not appear explicitly, and hence flows do only depend on $\eta_{A,k}$, the vertex couplings g, masses and further couplings. Note that this is only partially due to the approximation in (38). It mainly relates to the parametrizations (35) of the vertices which store most of the nontrivial information in the associated vertex couplings

$$\alpha_i = \frac{g_i^2}{4\pi}, \quad \text{with} \quad i = \bar{c}Ac, \qquad A^3, \quad A^4, \quad \bar{q}Aq. \tag{46}$$

This freedom directly relates to the reparametrization invariance of the theory and hence to RG invariance. The above discussion in particular applies to the anomalous dimension itself. First, we note that the glue part $\eta_{{\rm glue},k}$ of the anomalous dimension $\eta_{A,k}$ only depends on the vertex couplings:

$$\eta_{{\rm glue},k} = \eta_{{\rm glue},k}(\alpha_{\bar{c}Ac}, \alpha_{A^3}, \alpha_{A^4}). \tag{47}$$

In the semiperturbative regime these couplings agree due to the (RG-)modified Slavnov-Taylor identities [7,30–32], which themselves do not restrict the couplings in the nonperturbative transition regime; see Ref. [3]. In turn, in the nonperturbative regime the couplings differ already due to their different scalings with the gluonic dressing

$Z_{A,k}$. For small cutoff scales $k \to 0$, this dressing diverges proportional to the QCD mass gap,

$$\lim_{k\to 0} Z_{A,k} \propto \bar{m}^2_{\rm gap} = \frac{m^2_{\rm gap}}{k^2}. \tag{48}$$

This is a slight abuse of notation since $\bar{m}^2_{\rm gap}$ in (48) is not renormalized as the other dimensionless mass ratios $\bar{m}^2$. Here it simply relates to the wave-function renormalization $Z_{A,k}$ defined in (40). Hence, it is not RG invariant and should not be confused with the physical mass gap of QCD. It is related with the latter upon an appropriate renormalization.

As a consequence, while we expect $\alpha_{\bar{c}Ac} \approx \alpha_{\bar{q}Aq}$ down to small scales, the purely gluonic couplings should be suppressed to compensate the higher powers of diverging $Z_{A,k}$ present in the vertex dressing in (35). This also entails that we may parametrize the right-hand side with powers of $1/\alpha_i$. For $i = \bar{c}Ac, \bar{q}Aq$, for example, we expect $1/\alpha_i$. In accordance with this observation, we parametrize the difference of the various vertex couplings in $\eta_{\rm glue}$ with the gap parameter $\bar{m}_{\rm gap}$ defined in (48) and conclude for the gluon anomalous dimension of QCD

$$\eta_{A,k} = \eta_{{\rm glue},k}(\alpha_s, \bar{m}_{\rm gap}) + \Delta\eta_{A,k}(\alpha_{\bar{q}Aq}, \bar{m}_q), \tag{49}$$

where α_s stands for either $\alpha_{\bar{c}Ac}$ or α_{A^3}. We shall check that our results do not depend on this choice which justifies the identification of the couplings in (49). Note that this does not entail that the couplings agree but that they differ only in the regime where the glue fluctuations decouple. Moreover, in the present approximation α_{A^4} is not computed separately but identified with α_{A^3}.

A simple reduction of (49) is given by

$$\eta_{A,k} = \eta^{\rm YM}_{A,k} + \Delta\eta_{A,k}(\alpha_{\bar{q}Aq}, \bar{m}_q). \tag{50}$$

This amounts to a gluon propagator, where the vacuum polarization is simply added to the Yang-Mills propagator. This approximation has been used in an earlier work, [1,2,10], and subsequently in related Dyson-Schwinger works; see e.g. [33–36].

The term $\Delta\eta_{A,k}$ is the quark contribution to the gluon anomalous dimension, and is computed with

$$\Delta\eta_{A,k} = \frac{Z^{-1}_{A,k}}{3(N_c^2-1)} \left(\frac{\partial^2}{\partial p^2} \Pi^{\perp}(p) \cdot \right) \Bigg|_{p=0} \tag{51}$$

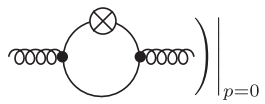

Here, p is the modulus of the external momentum and $\Pi^{\perp}$ is the transversal projection operator defined in (C2). Note that the dots represent full vertices and the lines stand for full propagators. The crossed circle represents the regulator insertion. For $N_f = 2$ and $N_c = 3$ we find

$$\Delta\eta_{A,k} = \frac{1}{24\pi^2} g^2_{\bar{q}Aq,k} (1+\bar{m}^2_{q,k})^{-4} \times [4 - \eta_{q,k} + 4\bar{m}^2_{q,k} - (1-\eta_{q,k})\bar{m}^4_{q,k}]. \tag{52}$$

The approximation (51) works well as long as the quark contribution has only a mild momentum dependence. This is the case due to the gapping of the quarks via spontaneous chiral symmetry breaking, and has been checked explicitly. A necessary check for the validity of this equation is that it reduces to the perturbative result in the corresponding limit, i.e. $\eta_{q,k}, \bar{m}_{q,k} \to 0$. Indeed, (52) reduces to 1-loop perturbation theory in this case, $\Delta\eta_{A,k} = g^2_{\bar{q}Aq,k}/(6\pi^2)$.

This leaves us with the task of determining $\eta_{{\rm glue},k}(\alpha_s, \bar{m}^2_{\rm gap})$, the pure glue contribution to $\eta_{A,k}$. The loop expression for $\eta_{\rm glue}$ only consists of Yang-Mills diagrams. As it depends solely on the value of the coupling α_s we arrive at

$$\eta_{\rm glue}(\alpha_s, \bar{m}^{\rm QCD}_{\rm gap}) = \eta^{\rm YM}_A(\alpha_s, \bar{m}^{\rm QCD}_{\rm gap}); \tag{53}$$

i.e. the pure gauge part of the gluon anomalous dimension of QCD is identical to the gluon anomalous dimension of pure Yang-Mills theory except it is driven by the QCD couplings. $\eta^{\rm YM}_A$ can be determined in Yang-Mills theory or in quenched QCD as a function of α_s and $\bar{m}_{\rm gap}$.

For using (53), a trackable form of $\eta^{\rm YM}_A$ as well as $\bar{m}^{\rm QCD}_{\rm gap}$ is required. To this end, we first note that $\eta(\alpha_{s,k})$ is a multivalued function in both Yang-Mills theory/quenched QCD and QCD; see Fig. 4. The two branches meet at $k = k_{\rm peak}$ (peak of the coupling) with

$$\partial_t \alpha_{s,k}|_{k=k_{\rm peak}} = 0. \tag{54}$$

We have a UV branch $\eta^+(\alpha_s, \bar{m}_{\rm gap})$ for $k > k_{\rm peak}$ and an IR branch $\eta^-(\alpha_s, \bar{m}_{\rm gap})$ for $k < k_{\rm peak}$. In Fig. 4 we show $\eta^{\rm YM}_A$ as a function of the coupling. Interestingly, $\eta^+(\alpha_{s,k})$ is well

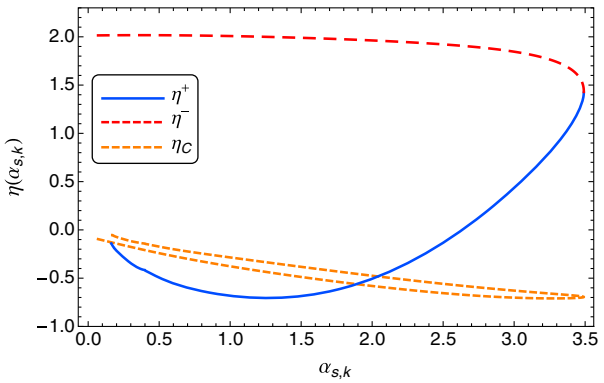

FIG. 4. The UV and IR branches of $\eta^{\rm YM}_A$, η^+ and η^-, as a function of the strong coupling.

described by a quadratic fit in α_s up to couplings close to $\alpha_{s,k_{\rm peak}}$. In turn, $\eta^-(\alpha_{s,k})$ is well described as a function of the cutoff scale as indicated by (48). In the deep IR the gluon dressing function is determined by the bare gap, $Z_{A,k\to 0} \propto m_{\rm gap}^2/k^2$; see also the discussion around (45). Hence we have

$$\lim_{k\to 0}\eta_{A,k} = 2. \tag{55}$$

This is seen in Fig. 4. We also see in this figure that the whole IR branch η^- is almost constant. This implies that the mass gap which suppresses $\alpha_{s,k}$ develops quickly around $k \approx k_{\rm peak}$ and remains roughly constant for the rest of the flow for $k \lesssim k_{\rm peak}$. This allows us to parametrize the IR-branch in terms of the RG scale,

$$\eta^- = 2 - c^- k^2, \quad \text{with} \quad c^- = \frac{2-\eta_A^{\rm YM}(\alpha_{\rm peak})}{k_{\rm peak}^2}, \tag{56}$$

where the mass gap $\bar{m}_{\rm gap}^2$ relates to $\eta_A^{\rm YM}(\alpha_{\rm peak})$. Note that the quality of these simple fits entails that the transition from the semiperturbative regime to the nonperturbative IR regime happens quite rapidly and asymptotic fits in both areas work very well. In summary we arrive at the final representation of $\eta_A^{\rm YM}$ with

$$\begin{aligned}\eta_{A,k}^{\rm YM}(\alpha_{s,k}) = {} & \eta^+(\alpha_{s,k})\theta(\alpha_{s,k}-\alpha_{s,\rm peak}) \\ & + \eta^-(k)\theta(\alpha_{s,\rm peak}-\alpha_{s,k}).\end{aligned} \tag{57}$$

Inserting (57) on the right-hand side of (53) gives us a closed equation for $\eta_{A,k}$ in (49). Its integration also provides us with the QCD mass gap.

The same analysis as for $\eta_{A,k}$ can be applied to the ghost anomalous dimension $\eta_{c,k}$ leading to a similar representation with the only difference that $\eta_{c,k=0} = 0$. It turns out that an even simpler global linear fit gives quantitatively reliable results for matter correlations,

$$\eta_{c,k}(\alpha_{s,k}) = \frac{\alpha_{s,k}}{\alpha \eta_{c,k}^{\rm YM}}(\alpha), \tag{58}$$

where $\alpha_{s,k} = \alpha_{\bar{c}Ac,k}$; see Fig. 4. This modification is used in the equation for the ghost-gluon vertex. Note that this overestimates ghost-gluon correlations in the deep infrared where the glue sector has decoupled from the matter sector. Hence this is of no relevance for the physics of chiral symmetry breaking discussed in the present work.

We are now in a position to finally determine the ghost and gluon propagators at vanishing cutoff scale in dynamical QCD. Again, we could use the $\alpha, \bar{m}_{\rm gap}$ representation for extracting the full dressing function $Z_{A,k}(p)$ on the basis of the results. To that end, the momentum-dependent flows as functions of $\alpha, \bar{m}_{\rm gap}$ are required:

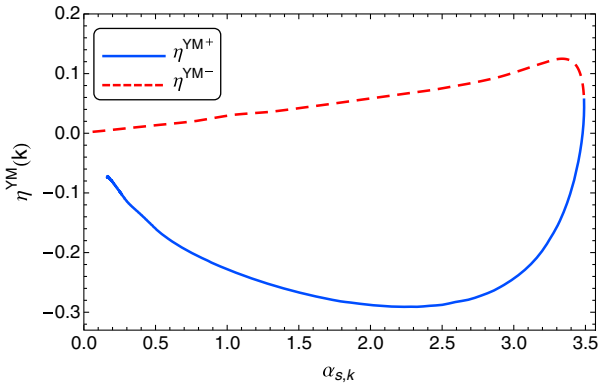

FIG. 5. The UV and IR branches of $\eta_{A,k}^{\rm YM}(k)$, which is defined in (59).

$$\eta_{A,k}^{\rm YM}(p) = -\frac{\partial_t Z_{A,k}^{\rm YM}(p)}{Z_{A,k}^{\rm YM}(p)}, \qquad \partial_t \Delta\eta_{A,k}(p), \tag{59}$$

where $\Delta\eta_{A,k}(p)$ stands for the momentum-dependent flow of the vacuum polarization. The first term in (59) again is well approximated in terms of a low order polynomial in α_s. This is expected because it relates directly to the standard anomalous dimension of the gluon. In Fig. 5 it is shown for momentum $p = k$ as a function of $\alpha_{s,k}$. The definition of $\eta_{A,k}^{\rm YM}(p)$ implies that only the first term in (42) contributes here. Thus, for vanishing k (44) holds and hence $\lim_{k\to 0}\eta_{A,k}^{\rm YM}(k) = 0$ as observed in Fig. 5.

An already very good estimate for the dressing function is

$$Z_{A,k=0}(p) \simeq Z_{A,k=p}(p) = Z_{A,k=p}, \tag{60}$$

as the flow of the propagators decays rapidly for momenta larger than the cutoff scale, $p \gtrsim k$. Moreover, the momentum derivative of the dressing is only large in the UV-IR transition regime. In Fig. 6, the inverse dressing $1/Z_{A,0}(p)$ and its approximation $1/Z_{A,p}$ are shown. Clearly, there are only minor deviations in the UV-IR transition regime. The same argument holds true to an even better degree for the quark contribution, and we have checked the smoothness of the flow $\Delta\Gamma_{A,k}(p)$. This leads to a very simple, but quantitative estimate for the full dressing function with

$$Z_{A/c,k=0}^{\rm glue}(p) \simeq \frac{Z_{A/c,k=0}^{\rm YM}(k_\alpha)}{Z_{A/c,k_\alpha}^{\rm YM}} Z_{A/c,k=p}^{\rm glue}, \tag{61}$$

with

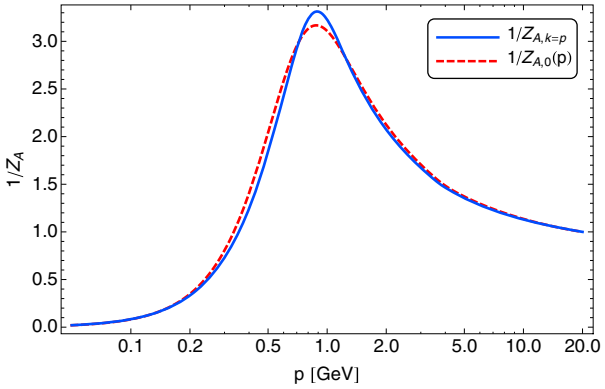

FIG. 6. Comparison of the momentum-dependent gluon dressing function $Z_{A,0}(p)$ and $Z_{A,k=p}$.

$$Z^{\text{glue}}_{A/c,k} = \exp\left\{-\int_\Lambda^p \frac{dk}{k}\eta^{\text{glue}}_{A/c,k}\right\}, \tag{62}$$

where $Z_{A/c,\Lambda} = 1$, and $k_\alpha = k(\alpha_{s,k})$ is the YM-cutoff value that belongs to a given coupling α_s.

In summary we conclude that, based on Fig. 6, an already quantitative approximation to the fully unquenched propagator is achieved by setting the ratio in (61) to unity. This leads to

$$Z_{A/c}(p) \simeq \exp\left\{-\int_\Lambda^p \frac{dk}{k}\eta_{A/c,k}\right\}, \tag{63}$$

with $\eta_{A/c,k}$ defined in (49). In the nonperturbative regime diagrams involving an internal gluon are suppressed with the generated gluon mass. Hence, albeit the approximation by itself may get less quantitative in the infrared, the error propagation in the computation is small.

In summary this leaves us with relatively simple analytic flow equations for the fully back-coupled unquenching effects of glue and ghost propagators. A full error analysis of the analytic approximations here will be published elsewhere, and is very important for the reliable application of the present procedure to finite temperature and density.

In the following, we will outline the definition and derivation of the gluonic vertices we use. First of all, we only take into account the classical tensor structure of the vertices. Moreover, throughout this work, we define the running coupling at vanishing external momentum. Together with our choice for the regulators, this has the advantage that the flow equations are analytical equations. In particular, loop-momentum integrations can be performed analytically. This approximation is semiquantitative as long as the dressing of the classical tensor structures does not show a significant momentum dependence, and the other tensor structures are suppressed.

This approximation is motivated by results on purely gluonic vertices (see Refs. [25,37–44]), which show nontrivial momentum dependencies only in the momentum region where the gluon sector already starts to decouple from the system. In turn, the tensor structures and momentum dependencies of the quark-gluon vertex are important; see the Dyson Schwinger equations studies [45–47] and the recent fully quantitative FRG study [3]. To take this effectively into account, we introduce an infrared-strength function for the strong couplings, which is discussed at the end of this section and in Appendix D.

To extract the flow of the quark-gluon coupling $g_{\bar{q}Aq}$, we use the following projection procedure,

$$\partial_t g_{\bar{q}Aq} = \frac{1}{8N_f(N_c^2-1)} \times \lim_{p\to 0}\text{Tr}\left(\gamma_\mu t^a \frac{\partial_t \Gamma_k}{\delta q \delta A^a_\mu \delta \bar{q}}\right)\Big|_{\Phi=\Phi_0}, \tag{64}$$

which leads to the equation

$$\begin{aligned}\partial_t g_{\bar{q}Aq,k} = {}& \frac{1}{2}(\eta_{A,k} + 2\eta_{q,k}) g_{\bar{q}Aq,k} \\ & - v(d) g_{\bar{q}Aq,k}\bar{h}_k^2 \{\mathcal{N}^{(m)}_{2,1}(\bar{m}^2_{q,k}, \bar{m}^2_{\sigma,k}; \eta_{q,k}, \eta_{\phi,k}) \\ & + (N_f^2-1)\mathcal{N}^{(m)}_{2,1}(\bar{m}^2_{q,k}, \bar{m}^2_{\pi,k}; \eta_{q,k}, \eta_{\phi,k})\} \\ & + g^3_{\bar{q}Aq,k}\frac{12v(d)}{N_c}\mathcal{N}^{(g)}_{2,1}(\bar{m}^2_{q,k}; \eta_{q,k}, \eta_{A,k}) \\ & + g^2_{\bar{q}Aq,k} g_{A^3,k} 3v(d) N_c \mathcal{N}^{(g)}_{1,2}(\bar{m}^2_{q,k}; \eta_{q,k}, \eta_{A,k}).\end{aligned} \tag{65}$$

The threshold functions appearing on the right-hand side can be found in Appendix C. For the quark-gluon vertex, no ghost diagrams are present. Furthermore, the mesonic contributions dominate in the infrared. These contributions have the same sign as the gluonic ones and therefore lead to an effective infrared enhancement of the quark-gluon vertex. The three-gluon vertex $g_{A^3,k}$ is defined via

$$\partial_t g_{A^3,k} = \frac{i}{12N_c(N_c^2-1)}\lim_{p\to 0}\frac{\partial^2}{\partial p^2} \times \text{Tr}\left(\delta_{\mu\nu} p_\sigma f^{abc}\frac{\partial_t \Gamma_k}{\delta A(p)^a_\mu \delta A(-p)^b_\nu \delta A^c_\sigma(0)}\right)\Big|_{\Phi=\Phi_0}. \tag{66}$$

Note that in the limit of vanishing external momentum the flow is independent of the kinematic configuration in the projection procedure. Thus, we find for the flow equation for $N_c = 3$ and $N_f = 2$

$$\partial_t g_{A^3,k} = \frac{3}{2}\eta_{A,k} g_{A^3,k} - \frac{1}{6\pi^2} g^3_{\bar{q}Aq,k}\left(1-\frac{\eta_{q,k}}{4}\right)\frac{(1+2\bar{m}^2_{q,k})}{(1+2\bar{m}^2_{q,k})^4} + \frac{3}{64\pi^2} g^3_{A^3,k}(11-2\eta_A) + \frac{1}{64\pi^2} g^3_{\bar{c}Ac,k}\left(1-\frac{\eta_{C,k}}{8}\right), \quad (67)$$

with the ghost anomalous dimension $\eta_{C,k} = -(\partial_t Z_{C,k}(k^2))/Z_{C,k}(k^2)$. The second line in (67) corresponds to the quark-triangle diagram and the third and fourth lines are the gluon- and ghost-triangle diagrams, respectively. Note that the third line also includes the contribution from the diagram containing the four-gluon vertex, which we approximate as explained below.

Within our approximation, the ghost-gluon vertex $g_{\bar{c}Ac,k}$ has only canonical running since the diagrams that contribute to the flow of $g_{\bar{c}Ac,k}$ are proportional to the external momentum. Thus, at vanishing external momentum they vanish and we are left with

$$\partial_t g_{\bar{c}Ac,k} = \left(\frac{1}{2}\eta_{A,k} + \eta_{C,k}\right) g_{\bar{c}Ac,k}. \quad (68)$$

Lastly, we comment on our approximation for the four-gluon vertex $g_{A^4,k}$. For the sake of simplicity, we restrict here to a semiperturbative ansatz for this vertex, which ensures that $g_{A^4,k}$ has the correct perturbative running. To this end, we set

$$g^2_{A^4,k} = g^2_{A^3,k}. \quad (69)$$

This approximation is valid for $k \gtrsim 1.5$ GeV. For smaller scales, nonperturbative effects potentially lead to a different running.

This leads to an explicit expression for $\Delta\Gamma_{\text{glue}}$ in (1):

$$\Delta\Gamma_{\text{glue}} = \int_x \left\{\frac{1}{4}(F^2|_{g_k=g_{A^3,k}} - F^2|_{g_k}) + \bar{c}^a\partial_\mu(D^{ab}_\mu|_{g_k=g_{\bar{c}Ac,k}} - D^{ab}_\mu|_{g_k})c^b + Z_{q,k}\bar{q}\gamma_\mu(D_\mu|_{g_k=g_{\bar{q}Aq,k}} - D_\mu|_{g_k})q\right\}, \quad (70)$$

where we used the abbreviation $F^2 = F^a_{\mu\nu}F^a_{\mu\nu}$. We see that $\Delta\Gamma_{\text{glue}}$ corrects for distinctive coupling strengths for interaction terms. While perturbation theory ensures that all couplings agree in the UV, nonperturbative effects lead to differing behavior in the midmomentum and IR regime.

The result for the different running couplings discussed here is shown in Fig. 7. While they all agree with each other and follow the perturbative running at scales $k \gtrsim 3$ GeV, nonperturbative effects induce different runnings at lower scales. In particular, the former statement is a highly nontrivial consistency check of the approximation we make here.

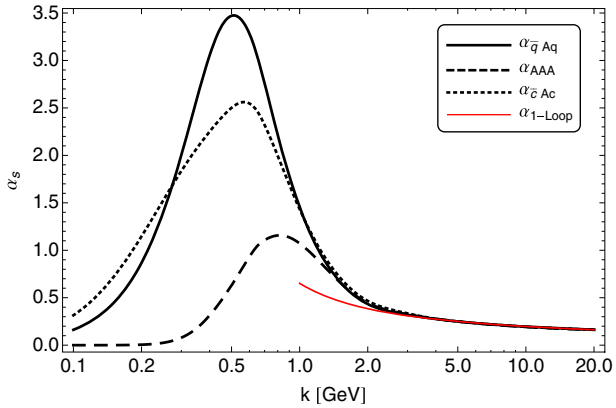

FIG. 7. The running of the different strong couplings in comparison to the 1-loop running. Since perturbation theory breaks down at the scale where the strong couplings start to deviate from each other, we show the 1-loop running only down to 1 GeV.

As discussed above, in the present study we focus on the RG flows of the most relevant couplings from a phenomenological point of view. In particular, we concentrate on the effects of fluctuations on the relevant and marginal parameters of the classical gauge action in (1). Consequently, nonclassical interactions which are potentially relevant are not taken into account here. Furthermore, we only consider vertices at vanishing external momenta, although momentum dependencies may play an important quantitative role. As an example, this becomes apparent in the flow of the ghost-gluon vertex (68): while the diagrams driving the flow of $g_{\bar{c}Ac,k}$ vanish within our approximation, they give finite contributions at nonvanishing momenta. This was studied in more detail in the case of quenched QCD [3]. Indeed, it turned out that both momentum dependencies and the inclusion of nonclassical vertices lead to large quantitative effects. It was shown there that within an extended truncation the approach put forward in the present work leads to excellent quantitative agreement with lattice QCD studies.

We take the findings in [3] as a guideline for a phenomenological modification of the gauge couplings. Effectively this provides additional infrared strength to the gauge couplings in the nonperturbative regime with $k \lesssim 2$ GeV. This additional strength is adjusted with the current quark mass at vanishing momentum. This is reminiscent of similar procedures within Dyson-Schwinger studies (see e.g. [16,17]); the details are given in Appendix D.

IV. RESULTS

First we summarize the system of flow equations used in the present work. The effective potential $\bar{V}_k(\bar{\rho})$ and the

Yukawa coupling $\bar{h}_k(\bar{\rho})$ are expanded about a fixed bare field as shown in (5). These expansions are already fully converged for $N_V = 5$ and $N_h = 3$; for a detailed discussion see [27]. The flow equations for the effective potential and its expansion coefficients are given by (B1) and (B2). For the Yukawa coupling they are given by (B6) and (B7) in the case of scale-independent meson fields. The latter are modified by dynamical hadronization which results in (33) for the final flow of the Yukawa coupling. The flows of the renormalized expansion point $\bar{\kappa}_k$ and the explicit symmetry breaking $\bar{c}_k$ are purely canonical and given by (B3). In order to accurately capture the physics in the IR, we choose the expansion point such that it matches the minimum of the renormalized effective potential at $k = 0$, $\bar{\kappa}_{k=0} = \bar{\rho}_{0,k=0}$; cf. [27] for details. Owing to dynamical hadronization, the flow of the four-quark interaction $\bar{\lambda}_{q,k}$ for scale-independent fields enters through the flow of the Yukawa coupling and is given by (B8). Following our construction discussed in Sec. III B, the flow of $\bar{\lambda}_{q,k}$ vanishes in the presence of the scale-dependent mesons. The RG flows of the quark-gluon, the three-gluon and the ghost-gluon couplings are given by (65), (67) and (68). Owing to our construction of the vertices [see (35)], nontrivial momentum dependencies of the propagators enter solely through the corresponding anomalous dimensions $\eta_{\Phi,k}$. For the mesons and quarks they are given by (B11) and (B13). The parametrization of the gluon and ghost anomalous dimensions is discussed in Sec. III C. The gluon anomalous dimension $\eta_{A,k}$ is defined by (49) and contains the pure gauge part and the vacuum polarization. The vacuum polarization is given by (52). The pure gauge part is constructed from the full gluon anomalous dimension of pure Yang-Mills theory, which we use as an input. It is computed from (53) and (57) with $\alpha_{s,k} = \alpha_{\bar{c}Ac,k}$. The ghost anomalous dimension of QCD is computed from (58), where we also augment the input from pure Yang-Mills theory by correcting for the differences between the strong couplings of YM and QCD, which, in turn, are computed here. Together with the fact that we evaluate all flows at vanishing external momentum, this leads to a set of ordinary differential equations in the RG scale k which can easily be solved.

The starting point of the present analysis is the microscopic action of QCD. We therefore initiate the RG flow at large scales, deep in the perturbative regime. The initial values for the strong couplings are fixed by the value of the strong coupling obtained from 1-loop perturbation theory. Since the different strong couplings we use here [see Eq. (46)] need to be identical in the perturbative regime, they consequently have the same initial value α_s. It is shown in Fig. 7 that indeed the different strong couplings agree to a high degree of accuracy with the 1-loop running of the strong coupling for scales $k > 3$ GeV. This is a very important benchmark for the consistency of the approximations we use. Note that the value of α_s implicitly determines the absolute physical scale. Here we choose $\alpha_{s,\Lambda} = 0.163$, which relates to $\Lambda \approx 20$ GeV. A quantitative determination requires the determination of the RG condition in relation to standard ones such as the $\overline{\text{MS}}$ scheme as well as the extraction of $\alpha_{s,k=0}(p = \Lambda)$, using Λ as the renormalization point. This goes beyond the scope of the present paper and we shall restrict ourselves to observables that are ratios of scales; our absolute scales are determined in terms of $\Lambda = 20$ GeV. The other microscopic parameter of QCD, the current quark mass, is in our case fixed by fixing the symmetry breaking parameter c. We choose $\bar{c}_\Lambda = 3.6\ \text{GeV}^3$ which yields an infrared pion mass of $M_{\pi,0} = 137$ MeV; $M_k = k\bar{m}_k$ is the renormalized dimensionful mass.

Note that the masses defined in Eq. (6), and hence in particular $M_{\pi,0}$, are curvature masses, i.e. the Euclidean two-point functions evaluated at vanishing momentum. However, it is the pole masses, defined via the poles of the propagators, that are measured in the experiments. Moreover, curvature and pole masses do not necessarily agree. In the present work, this difference is potentially of importance for the accurate determination of the pion mass. Now we use that curvature and pole masses are close for weakly momentum-dependent wave-function renormalizations; for a detailed discussion see [48]. There it also has been shown that the pion wave-function renormalization is indeed weakly momentum dependent, and pion curvature and pole mass deviate by less than 1%. It has been also shown in [48] that the large deviation of pion pole and curvature masses seen in previous works, [49], originates in the local potential approximation (LPA). Moreover, a scale-dependent, but momentum-independent, wave-function renormalization already removes the discrepancies seen in LPA, and the results agree well within the 1% level. In summary, curvature and pole mass of the pion agree on the 1% level. The inclusion of momentum-independent running wave-function renormalizations, as in the present work, guarantees quantitative reliability for this issue.

Since mesons are not present in the perturbative regime, we only have to make sure that this sector is decoupled at the initial scale. We therefore choose $M^2_{\pi,\Lambda} = M^2_{\sigma,\Lambda} = 10^4\Lambda^2$. Our results are independent of the choice of the initial masses and the Yukawa coupling as long as the initial four-fermi coupling related to it is far smaller than α_s^2. This is demonstrated for the Yukawa coupling in Fig. 8, where we see that, with initial values that differ by many orders of magnitude, we always get the same solution in the IR. Loosely speaking, the memory of the initial conditions is lost in the RG flow towards the IR regime due to the presence to a pseudofixed point on intermediate scales; see also Ref. [23].

In the present work we have studied the unquenching effects due to the full back-coupling of the matter dynamics to the glue sector. In earlier work [2,10], we directly identified $\eta_{\text{glue},k} = \eta^{\text{YM}}_{A,k}$ at the same cutoff scale k; see

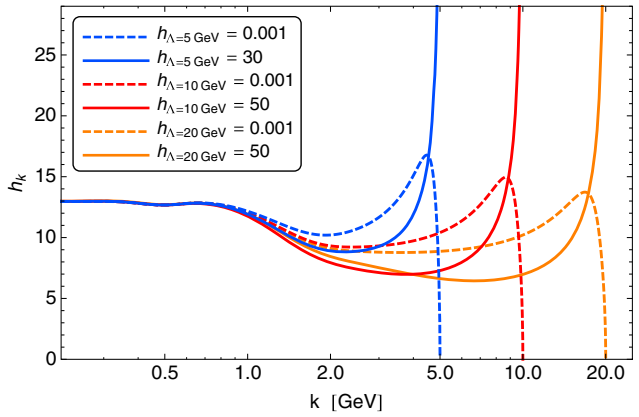

FIG. 8. Yukawa coupling as a function of the RG scale for various initial scales Λ and initial conditions h_Λ.

Eq. (50). This simply adds the vacuum polarization to the Yang-Mills propagator without feedback. It is well adapted for taking into account qualitatively even relatively large matter contributions to the gluonic flow: the main effect of the matter back-coupling is the modification of scales, most importantly Λ_{QCD}, which is already captured well in (1-loop) perturbation theory, if the initial scale is not chosen to be too large. This approximation has also been subsequently used in related Dyson-Schwinger works (see e.g. [33–36]), extending the analysis also to finite density. Here, we improve these approximations by taking into account the backreaction of matter fluctuations on the pure gauge sector. Furthermore, the gluon vacuum polarization was based on a 1-loop improved approximation in previous FRG studies. Here, we compute the full vacuum polarization self-consistently.

In Fig. 9 we show the quenched and unquenched gluon propagators. The quenched gluon propagator is a FRG input from [18,26]. We clearly see that the screening effects

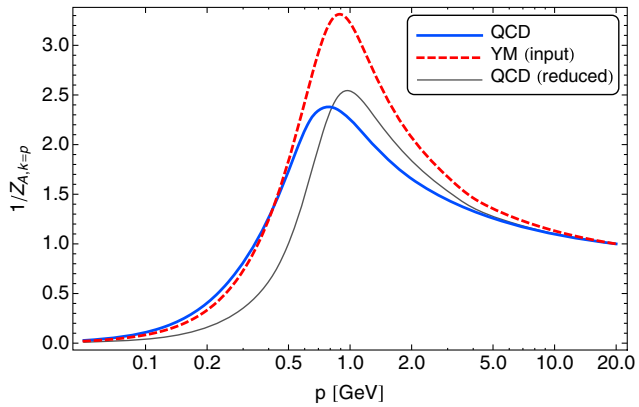

FIG. 9. Comparison between the quenched and the unquenched running gluon propagators $1/Z^{\mathrm{YM}}_{A,k}(k^2)$ and $1/Z_{A,k}(k^2)$ as defined in Eq. (61). We also show the curve for QCD (reduced) where the gluon propagator is a direct sum of Yang-Mills propagator and vacuum polarization; see Eq. (50).

of dynamical quarks decrease the strength of the gluon propagator. Figure 9 also shows the partially unquenched results [denoted by "QCD (reduced)" in Fig. 9] for the propagator. Here, partially unquenched refers to an approximation, where the gluon propagator is a direct sum of Yang-Mills propagator and vacuum polarization; see Eq. (50). It shows deviations from the fully unquenched computation. This is seemingly surprising as it is well tested that partial unquenching works well even at finite temperature; see e.g. [2,10,33–36]. However, we first notice that the importance of quark fluctuations is decreased at finite temperature due to the Matsubara gapping of the quarks relative to the gluons. This improves the reliability of the partial unquenching results. Moreover, in these works the infrared strength is phenomenologically adjusted with the constituent quark mass in the vacuum. This effectively accounts for the difference between unquenching and partial unquenching. Note that this finding rather supports the stability and predictive power of functional approaches.

On the other hand this also entails that the full unquenching potentially is relevant in situations where the vacuum balance between pure glue fluctuations and quark fluctuations is changed due to an enhancement of the quark fluctuations. Prominent cases are QCD with a large number of flavors, and in particular QCD at finite density. Indeed, (49) even shows the self-amplifying effect at large quark fluctuations: the sign of the correction by $\Delta\eta_{A,k}$ is such that when it grows large, the ratio $\alpha_{s,\mathrm{QCD}}/\alpha_{s,\mathrm{YM}}$ decreases as does η_{glue} and the importance of the matter fluctuations is further increased. A more detailed study of this dynamics in the above-mentioned situations has been deferred to a subsequent publication.

Using the same parameters as in Ref. [3], we compare the quenched and unquenched quark propagators in Fig. 10. As for the gluon propagator, Fig. 9, we see large unquenching effects. Unquenching results in smaller quark masses (blue

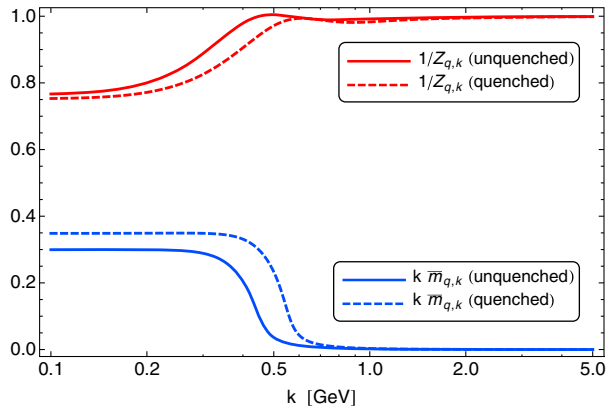

FIG. 10. Dressing function (red) and mass (blue) of the quark as function of the RG scale at vanishing momentum. We compare our present model (solid) to the quenched model (dashed) with the parameters fixed to match those of [3].

lines) and larger wave-function renormalizations $Z_{q,k}$, and, therefore, enhanced quark fluctuations, as expected. Furthermore, we see that the generation of constituent quark masses takes place at smaller scales in the unquenched case. This can again be traced back to screening effects: the effects of gauge fluctuations are suppressed in the presence of dynamical quarks and lead to weaker gauge couplings. Since the strength of the gauge couplings triggers chiral symmetry breaking, criticality of the four-quark interactions is reached later in the flow for weaker gauge couplings. Hence, chiral symmetry breaking takes place at smaller scales in the presence of dynamical quarks.

The results for the different running gauge couplings $\alpha_{\bar{q}Aq}$, $\alpha_{\bar{c}Ac}$ and α_{A^3} discussed in Sec. III C are shown in Fig. 7. At scales $k \gtrsim 3$ GeV they agree with the perturbative running. This constitutes a nontrivial consistency of the present computation. At lower scales, nonperturbative effects induce different runnings.

The different strengths of the gauge couplings in the nonperturbative regime are a direct consequence of the mass gap that develops in the gluon dressing function $Z_{A,k}$. Owing to our construction for the vertices and the gluon propagator, (35) and (38), all nontrivial information about the gauge sector is encoded in the gauge couplings. In particular, they genuinely involve powers of $Z_{A,k}^{1/2}$ that correspond to the number of external gluon legs attached to them. Hence, the more external gluonic legs the coupling has, the more its strength is suppressed by the emerging gluon mass gap. This explains why the three-gluon vertex α_{A^3} is much weaker in the nonperturbative regime than $\alpha_{\bar{q}Aq}$ and $\alpha_{\bar{c}Ac}$: it is suppressed by $Z_{A,k}^{3/2}$, while the quark-gluon and ghost-gluon couplings are only suppressed by $Z_{A,k}^{1/2}$. The gluon dressing function as we defined it here diverges for $k \to 0$, and, thus, all gauge couplings become zero in this limit.

The fact that $\alpha_{\bar{c}Ac}$ is weaker than $\alpha_{\bar{q}Aq}$ can be attributed to the neglected momentum dependencies in this sector. Since all diagrams that drive the flow of the ghost-gluon vertex are proportional to the external momentum, they vanish for our approximation and $\alpha_{\bar{c}Ac}$ only runs canonically; see (68). If these momentum dependencies were taken into account, the ghost-gluon vertex would even be stronger than the quark-gluon vertex, at least in the quenched case [3].

The present approach allows easy access to the relative importance of quantum fluctuations of the respective fields: we find that for the renormalized, dimensionless mass being larger than one,

$$\bar{m}_\Phi^2 = \frac{m_\Phi^2}{Z_\Phi k^2} \geq 1, \tag{71}$$

all threshold functions that depend on the propagator of the respective field mode are suppressed with powers of $1/\bar{m}_\Phi^2$. This entails that the dynamics of the system is not sensitive to fluctuations of this field. In turn, for $\bar{m}_\Phi^2 \leq 1$ the field mode is dynamical. Note that, of course, $\bar{m}_\Phi^2 = 1$ is not a strict boundary for the relevance of the dynamics. In Figs. 11 and 12 we show $\bar{m}_\Phi^2$ for the matter fields. In the shaded area the condition (71) applies, and the respective matter fields do not contribute to the dynamics. This already leads to the important observation that the resonant mesonic fluctuations are only important for the dynamics in a small momentum regime with momenta $p^2 \lesssim 800$ MeV; see also Fig. 12. While the σ and quark modes decouple rather quickly at about 300–400 MeV, the $\vec{\pi}$ as a pseudo-Goldstone mode decouples at its mass scale of about 140 MeV.

In turn, in the ultraviolet regime, the mesonic modes decouple very rapidly; see Fig. 12 for the size of the propagator measured in units of the cutoff. At about 800 MeV this ratio is already 0.1. Above this scale the mesonic modes are not important, and QCD quickly is well described by quark-gluon dynamics without resonant

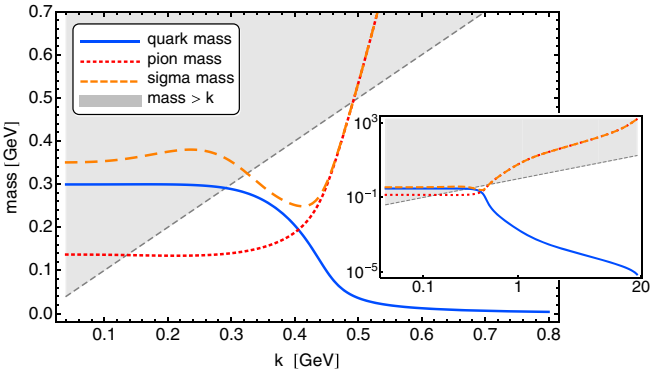

FIG. 11. The renormalized quark, pion and sigma masses as a function of the RG scale. The inset figure shows the masses for a larger range of scales. The shaded gray area indicates which fields contribute dynamically: masses within the gray area exceed the cutoff scale and the corresponding fields are therefore decoupled from the dynamics. On the other hand, fields with masses within the white area are dynamical.

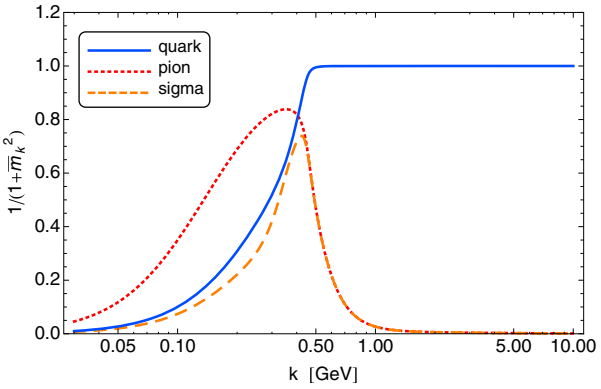

FIG. 12. Dimensionless RG-invariant propagators as functions of the RG scale.

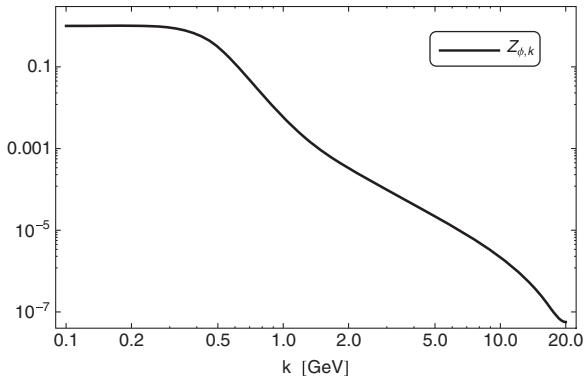

FIG. 13. Wave-function renormalization of the mesons.

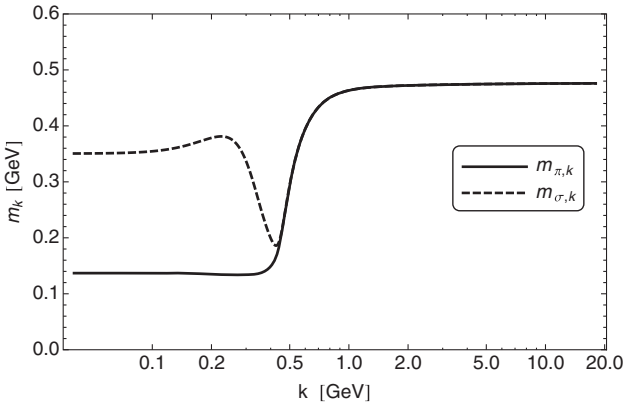

FIG. 14. The masses $m_{\pi/\sigma,k} = \sqrt{\Gamma^{(2)}_{\sigma/\pi}(0)} = kZ^{1/2}_{\phi,k}\bar{m}_{\pi/\sigma,k}$ of the mesons.

interactions. This observation is complementary to the fact that the initial condition of the Yukawa coupling does not play a role for the physics at vanishing coupling; see Fig. 8. For all initial cutoff scales $\Lambda \gtrsim 5$ GeV, its initial value is washed out rapidly, leading to a universal infrared regime with the prediction of $\bar{h}$ at $k = 0$.

We add that the Yukawa coupling relates to the ratio between constituent quark mass and the vacuum expectation value of the field $\bar{\sigma}$,

$$\bar{h} = \frac{\bar{m}_q}{\bar{\sigma}_0}. \tag{72}$$

Note that it cannot be tuned and is a prediction of the theory. On the other hand, in low-energy model studies, the (renormalized) quantities $\bar{m}_q$ and $\bar{\sigma}_0$ corresponding to physical observables are related to model parameters, and have to be tuned such that $\bar{m}_q$ and $\bar{\sigma}_0$ assume their physical values.

The decoupling of meson degrees of freedom is also reflected in the behavior of the meson wave-function renormalization $Z_{\phi,k}$ shown in Fig. 13. Starting at scales $k > 500$ MeV, $Z_{\phi,k}$ decreases very rapidly towards the UV. There, it is about seven orders of magnitude smaller than in the hadronic regime, where it is $\mathcal{O}(1)$. Furthermore, the masses $m^2_{\pi/\sigma,k} = \Gamma^{(2)}_{\sigma/\pi}(p^2 = 0) = Z_{\phi,k}M^2_{\pi/\sigma,k}$ become scale independent for $k > 800$ MeV as shown in Fig. 14. This implies that the meson sector becomes trivial beyond this scale. We see that the drastic decrease of the meson wave-function renormalization triggers the large renormalized meson masses $M^2_{\pi/\sigma,k} = m^2_{\pi/\sigma,k}/Z_{\phi,k}$ shown in Fig. 11, which are responsible for the suppression of the dynamics of the meson sector at scales $k > 800$ MeV. In turn, this implies that if we start with decoupled mesons in the UV as in the present case, i.e. initial meson masses much larger than the cutoff, the running of $Z_{\phi,k}$ drives the meson masses to their small values in the IR. Without this peculiar behavior of the meson wave-function renormalization, the meson masses would never become smaller than the cutoff scale and hence meson dynamics could not be generated dynamically. The fact that our results are independent of the exact value of the initial renormalized meson mass $M_{\phi,\Lambda} \gtrsim \Lambda$ implies that the running of $Z_{\phi,k}$ depends on the initial value $M_{\phi,\Lambda}$. Indeed, if we choose an initial meson mass that is one order of magnitude smaller (larger), $Z_{\phi,k}$ falls off by two orders of magnitude less (more). This is a direct consequence of the definition of the renormalized mass [cf. (28) with $M_k = k\bar{m}_k$] and the observation that the running of the meson masses is exclusively driven by $Z_{\phi,k}$ in the UV (cf. Fig. 14). Note that this behavior of $Z_{\phi,k}$ has consequences also for low-energy models in the local potential approximation, since for scales larger than about 800 MeV, the effect of running wave-function renormalizations cannot be neglected.

Finally, we discuss further consequences of our findings for low-energy effective models. To that end we note that the gluon modes decouple at momenta below 500–700 MeV. This is seen from the plot of the gluon dressing functions, Fig. 9, as well as that of the gluonic couplings in Fig. 7. This overlaps with the scale regime where the mesonic degrees of freedom start to dominate the dynamics.

Consequently, low-energy effective models aiming at quantitative precision that do not take into account any glue fluctuations should be initiated at a UV scale of about 500 MeV. In this regime, however, the quark-meson sector of QCD carries already some fluctuation information in nontrivial mesonic and quark-meson couplings. In other words, the standard initial effective Lagrangian of these models has to be amended by additional couplings. These couplings, however, can be computed from QCD flows.

It has been shown in [48] that in these low-energy effective models thermal fluctuations affect the physics at surprisingly large scales; for thermodynamical consequences, see Ref. [50]. This occurs even more so for density fluctuations that lack the exponential suppression present for thermal fluctuations. Thus, we conclude that the

low UV cutoff scale for quantitatively reliable low-energy effective models enforces the computation of temperature- and density-dependent initial conditions. Indeed the same argument holds true for other external parameters such as the magnetic field.

V. CONCLUSIONS AND OUTLOOK

In the present work, we have set up a nonperturbative FRG approach to QCD, concentrating on the effects of a full unquenching of the glue sector. We also provided a detailed study of the fluctuation physics in the transition region from the quark-gluon regime to the hadronic regime. This includes a discussion of the relative importance of the fluctuations of quark, meson and glue fluctuations. A detailed discussion is found in the previous section.

Here we simply summarize the main results. Firstly, we have shown that the full back-coupling of the matter fluctuations in the glue sector also plays a quantitative role in the vacuum. In the present two-flavor case, it accounts for about 10%–15% of fluctuation strength in the strongly correlated regime at about 1 GeV. This hints strongly at the importance of these effects in particular at finite density, where the importance of quark fluctuations is further increased and the effect is amplified.

Secondly, the still qualitative nature of the present approximation necessitates the adjustment of the infrared coupling strength, fixed with the constituent quark mass. However, the inclusion of dynamical hadronization which reenforces the four-fermion running, this phenomenological tuning is much reduced. In future work we plan to utilize the findings of the quantitative study [3] in quenched QCD for improving our current approximation towards quantitative precision, while still keeping its relative simplicity.

Finally, we have also discussed how low-energy effective models emerge dynamically within the present setup due to the decoupling of the glue sector: the present results and their extensions can be used to systematically improve the reliability of low-energy effective models by simply computing the effective Lagrangian of these models at their physical UV cutoff scale of about 500–700 MeV. Moreover, the temperature and density dependence of the model parameters at this UV scale can be computed within the present setup.

Future work aims at a fully quantitative unquenched study by also utilizing the results of [3], as well as studying the dynamics at finite temperature and density.

ACKNOWLEDGMENTS

We are grateful to Lisa M. Haas for many discussions and collaboration in an early stage of the project. We thank Tina Herbst, Mario Mitter and Nils Strodthoff for discussions and collaboration on related projects. J. B. acknowledges support by HIC for FAIR within the LOEWE program of the State of Hesse. Moreover, this work is supported by the Helmholtz Alliance HA216/EMMI and by ERC-AdG-290623. L. F. is supported by the European Research Council under the Advanced Investigator Grant No. ERC-AD-267258.

APPENDIX A: DYNAMICAL HADRONIZATION AND LOW-ENERGY EFFECTIVE MODELS

In low-energy models of QCD, such as (Polyakov-loop enhanced) Nambu-Jona-Lasinio models or quark-meson models, gluons are considered to be integrated out and one is left with effective four-quark interactions, either explicitly or in a bosonized formulation. The latter is particularly convenient as the phase with spontaneous broken chiral symmetry is easily accessible. There, the formulation of the effective theory is usually based on the conventional Hubbard-Stratonovich bosonization rather than dynamical hadronization. Following our arguments given in Sec. III A, the question arises whether dynamical hadronization leads to quantitative and/or qualitative corrections in the context of a low-energy effective model.

Since the matter part of our truncation (1) is that of a quark-meson model, we will consider here the special case of the quark-meson model defined by switching off all gluon contributions in (1). To see the effect of dynamical hadronization, we look at the ratios of IR observables obtained with and without dynamical hadronization. To this end, we choose $\Lambda_{\mathrm{LE}} = 1$ GeV as a typical UV-cutoff scale and use the same set of initial conditions in both cases. For results see Table I.

We see that the effect of dynamical hadronization on physical observables of a low-energy quark-meson model (without gluons) is negligible, since it only gives corrections of less than 1%. This does not change if we vary the UV-cutoff within the range of typical values for these types of models, i.e. $\Lambda_{\mathrm{LE}} \in [0.5, 1.5]$ GeV. Furthermore, it implies in particular that the miscounting problem discussed in Sec. III A is less severe in low-energy models.

This observation can be understood by looking at the flow of the four-quark interaction $\lambda_{q,k}$; see Eq. (B8). In the case of the quark-meson model, only the meson box diagrams $\sim h_k^4$ contribute to the flow (see also Fig. 1), while the gluon box diagrams are neglected. In the chirally symmetric regime, the mesons are decoupled and the corresponding contributions to the flow are therefore suppressed. Furthermore, in the hadronic regime, the quarks acquire a large constituent mass and, in addition, the pions

TABLE I. Effect of dynamical hadronization on a quark-meson model: the quantities with/without a tilde are the results obtained from a solution of the flow equations of the quark-meson model with/without dynamical hadronization techniques.

$f_\pi/\tilde{f}_\pi$	$M_q/\tilde{M}_q$	$M_\pi/\tilde{M}_\pi$	$M_\sigma/\tilde{M}_\sigma$
0.995	0.997	1.003	0.990

become light. Therefore, the contribution from dynamical hadronization to the flow of the Yukawa coupling (33), $\sim\bar{m}^2_{\pi,k}\partial_t\bar{\lambda}_{q,k}$, is suppressed by these two effects in the broken regime. Thus, following our present results, in particular Fig. 11, the only regime where dynamical hadronization can play a role in a low-energy model is in the vicinity of the chiral symmetry breaking scale. However, since this region is small compared to the range of scales considered even in low-energy models, only very small corrections related to the regeneration of four-quark interactions are accumulated from the RG flow.

Note, however, that we checked this statement only in vacuum and it might not be true in medium, especially at large chemical potential where quark fluctuations are enhanced. This can potentially lead to larger, non-negligible corrections from dynamical hadronization. We also emphasize that we used the same initial conditions for our comparison of the RG flow of the quark-meson model with and without dynamical hadronization techniques. However, usually the parameters of low-energy models are fixed in the vacuum, independent of the model truncation. Once the parameters are fixed, these models are then used to compute, e.g., the phase diagram of QCD at finite temperature and chemical potential. In this case, it may still very well be that the use of dynamical hadronization techniques yield significant corrections.

APPENDIX B: FLOW EQUATIONS OF THE COUPLINGS

In this appendix, we briefly discuss the derivation of the flow equations of the couplings before dynamical hadronization techniques are applied.

We expand the effective potential and the Yukawa coupling about a fixed expansion point κ; see (5). The advantage of such an expansion is that it is numerically stable, inexpensive and it converges rapidly [27]. This allows us to take the full field-dependent effective potential $V_k(\rho)$ and Yukawa coupling $h_k(\rho)$ into account in the present analysis.

The flow equation of the effective potential including the symmetry breaking source, $V_k(\rho)-c\sigma$, is obtained by evaluating (9) for constant meson fields, $\phi(x)\to\phi$ and vanishing gluon, quark and ghost fields. In this case, the effective action reduces to $\Gamma_k=\Omega^{-1}(V_k(\rho)-c\sigma)$, where Ω is the space-time volume. The flow of the effective potential $\bar{V}_k(\bar{\rho})=V_k(\rho)$ is then given by

$$\partial_t|_\rho\bar{V}(\bar{\rho})=2k^4v(d)\{[(N_f^2-1)l_0^B(\bar{m}^2_{\pi,k};\eta_{\phi,k})+l_0^B(\bar{m}^2_{\sigma,k};\eta_{\phi,k})]-4N_fN_cl_1^F(\bar{m}^2_{q,k};\eta_{q,k})\},\tag{B1}$$

where $v(d)=(2^{d+1}\pi^{d/2}\Gamma(d/2))^{-1}$ and the threshold functions l_1^B and l_1^F are given in Eq. (C4). The flows of the couplings in (5) can be derived from the above equation via

$$\partial_{\bar{\rho}}^n\partial_t|_\rho\bar{V}(\bar{\rho})|_{\bar{\rho}=\bar{\kappa}_k}=(\partial_t-n\eta_{\phi,k})\bar{\lambda}_{n,k}-\bar{\lambda}_{n+1,k}(\partial_t+\eta_{\phi,k})\bar{\kappa}_k.\tag{B2}$$

Rescaling the expansion point and the symmetry breaking source in order to formulate RG-invariant flows introduces a canonical running for these parameters:

$$\partial_t\bar{\kappa}_k=-\eta_\phi\bar{\kappa}_k,\qquad\partial_t\bar{c}=\frac{1}{2}\eta_\phi\bar{c}.\tag{B3}$$

The renormalized minimum of the effective potential $\bar{\rho}_{0,k}=\bar{\sigma}^2_{0,k}/2$, which determines the pion decay constant at vanishing IR cutoff, $\bar{\sigma}_{0,k=0}=f_\pi$, and serves as an order parameter for the chiral phase transition, is obtained from

$$\partial_{\bar{\rho}}[\bar{V}_k(\bar{\rho})-\bar{c}_k\bar{\sigma}]|_{\bar{\rho}_{0,k}}=0.\tag{B4}$$

All physical observables such as f_π and the masses are defined at vanishing cutoff scale $k=0$ and at the minimum of the effective potential $\bar{\rho}=\bar{\rho}_{0,k=0}$.

We define the field-dependent Yukawa coupling via the relation $m_{q,k}(\rho)=\sigma h_k(\rho)$ at vanishing external momentum and constant meson fields, leading to the following projection:

$$\partial_t h_k(\rho)=-\frac{1}{\sigma}\frac{i}{4N_cN_f}\lim_{p\to0}\mathrm{Tr}\left(\frac{\delta^2\partial_t\Gamma_k}{\delta q(-p)\delta\bar{q}(p)}\right)\Big|_{\rho(x)=\rho}.\tag{B5}$$

The resulting flow is given by

$$\begin{aligned}\partial_t|_{\bar{\rho}}\bar{h}(\bar{\rho})=&\left(\eta_{q,k}+\frac{1}{2}\eta_{\phi,k}\right)\bar{h}_k(\bar{\rho})-v(d)\bar{h}_k(\bar{\rho})^3[(N_f^2-1)L_{1,1}^{(FB)}(\bar{M}^2_{q,k},\bar{m}^2_{\pi,k};\eta_{q,k},\eta_{\phi,k})-L_{1,1}^{(FB)}(\bar{m}^2_{q,k},\bar{m}^2_{\sigma,k};\eta_{q,k},\eta_{\phi,k})]\\&+8v(d)\bar{h}_k(\bar{\rho})\bar{h}'_k(\bar{\rho})\bar{\rho}[\bar{h}_k(\bar{\rho})+2\bar{\rho}\bar{h}'_k(\bar{\rho})]\times L_{1,1}^{(FB)}(\bar{m}^2_{q,k},\bar{m}^2_{\sigma,k};\eta_{q,k},\eta_{\phi,k})\\&-2v(d)k^2[(3\bar{h}'_k(\bar{\rho})+2\bar{\rho}\bar{h}''_k(\bar{\rho}))l_1^B(\bar{m}^2_{\sigma,k};\eta_{\phi,k})+3\bar{h}'_k(\bar{\rho})l_1^B(\bar{m}^2_{\pi,k};\eta_{\phi,k})]\\&-8(3+\xi)C_2(N_c)v(d)g^2_{\bar{q}Aq,k}\bar{h}_k(\bar{\rho})\times L_{1,1}^{(FB)}(\bar{m}^2_{q,k},0;\eta_{q,k},\eta_{A,k}).\end{aligned}\tag{B6}$$

ξ is the gauge-fixing parameter, which we set to zero since we use the Landau gauge in this work. The function $L^{(FB)}_{1,1}$ is given in Eq. (C5). The flows of the renormalized couplings in (5) are

$$\partial^n_{\bar\rho}\partial_t|_\rho \bar h(\bar\rho)|_{\bar\rho=\bar\kappa_k} = (\partial_t - n\eta_{\phi,k})\bar h_{n,k} - \bar h_{n+1,k}(\partial_t+\eta_{\phi,k})\bar\kappa_k. \tag{B7}$$

It was shown in Ref. [27] already that a ϕ^4 expansion of the effective potential, corresponding to $N_V = 2$ in (5), gives quantitatively precise results for small temperatures and densities. On the other hand, a leading order expansion of the Yukawa coupling, i.e. $N_h = 0$, is not sufficient since the expansion has not yet converged. Here, we choose $N_h = 3$ to ensure that we take the effect of the full field-dependent Yukawa coupling into account. Note that we have to choose $N_V \geq N_h$ for numerical stability and therefore choose $N_V = 5$.

For the flow of the four-quark coupling we choose the projections in [12]. This yields

$$\begin{aligned}\partial_t\bar\lambda_{q,k} = &-g^4_{\bar qAq,k}\left(\frac{2N_c^2-3}{N_c}\right)v(d)L^{(FB)}_{1,2}(\bar m^2_{q,k};\eta_{q,k},\eta_{A,k})\\ &+\bar h_k(\bar\kappa_k)^4\left(\frac{2}{N_c}+1\right)v(d)\\ &\times L^{(FB)}_{1,1,1}(\bar m^2_{q,k},\bar m^2_{\pi,k},\bar m^2_{\sigma,k};\eta_{q,k},\eta_{\phi,k}).\end{aligned} \tag{B8}$$

The threshold functions $L^{(FB)}_{1,2}$ and $L^{(FB)}_{1,1,1}$ are shown in Eq. (C5). In Eq. (B8), we anticipate full dynamical hadronization for the four-fermi interaction. This leads to a vanishing four-quark coupling $\bar\lambda_{q,k} = 0$ on the right-hand side: the self-coupling diagram proportional to $\bar\lambda^2_{q,k}$ is dropped. Furthermore, we neglect contributions from higher order quark-meson vertices related to field derivatives of $\bar h_k(\bar\rho)$, since they are subleading.

The anomalous dimensions are related to the flow of the wave-function renormalizations, $\eta = -\partial_t Z/Z$. The Z's on the other hand encode the nontrivial momentum dependence of the propagators. Here, as already discussed above, we approximate the full momentum, scale and field dependence of the anomalous dimensions by only scale-dependent ones in the leading order expansion in the fields in analogy to (5):

$$Z_{\phi,k}(p^2,\rho) = Z_{\phi,k}(\kappa) \text{ and } Z_{q,k}(p^2,\rho) = Z_{q,k}(\kappa). \tag{B9}$$

For the meson anomalous dimension, we therefore use the following projection:

$$\eta_{\phi,k} = -\frac{1}{2Z_{\phi,k}}\lim_{p\to0}\frac{\partial^2}{\partial|p|^2}\mathrm{Tr}\left(\frac{\delta^2\partial_t\Gamma_k}{\delta\pi_i(-p)\delta\pi_i(p)}\right)\Big|_{\rho=\kappa}, \tag{B10}$$

where the choice of $i = 1, 2, 3$ does not matter, owing to the $O(3)$ symmetry of the pions. This yields

$$\begin{aligned}\eta_{\phi,k} = &\,8v(d)k^{-2}\bar\kappa_k\bar U'_k(\bar\kappa_k)^2\mathcal{M}_{2,2}(\bar m^2_{\pi,k},\bar m^2_{\sigma,k})\\ &+2N_cN_fv(d)\bar h_k(\bar\kappa_k)^2[\mathcal{M}_4(\bar m^2_{q,k};\eta_{q,k})\\ &+\frac{1}{2}k^{-2}\bar\kappa_k\bar h_k(\bar\kappa_k)^2\mathcal{M}_2(\bar m^2_{q,k};\eta_{q,k})].\end{aligned} \tag{B11}$$

The functions $\mathcal{M}_{2,2}$ and $\mathcal{M}_{2/4}$ are defined in Eq. (C6). Note that it is crucial that the functional derivatives in (B10) are with respect to the pions, since sigma-derivatives would contaminate the flow with contributions proportional to $\sigma Z'_{\phi,k}(\rho)$.

For the anomalous dimension of quarks, we use the projection

$$\begin{aligned}\eta_{q,k} = &-\frac{1}{8N_fN_cZ_{q,k}}\\ &\times\lim_{p\to0}\frac{\partial^2}{\partial|p|^2}\mathrm{Tr}\left(\gamma_\mu p_\mu\frac{\delta^2\partial_t\Gamma_k}{\delta q(-p)\delta\bar q(p)}\right)\Big|_{\rho=\kappa},\end{aligned} \tag{B12}$$

which yields

$$\begin{aligned}\eta_q = &\,2v(d)C_2(N_c)g^2_{\bar qAq}[(3-\xi)\mathcal{M}_{1,2}(\bar m^2_{q,k},0;\eta_{A,k})\\ &-3(1-\xi)\tilde{\mathcal{M}}_{1,1}(\bar m^2_{q,k},0;\eta_{q,k},\eta_{A,k})]\\ &+\frac{1}{2}v(d)[(\bar h_k(\bar\kappa_k)+2\bar\kappa_k\bar h'_k(\bar\kappa_k))^2\\ &\times\mathcal{M}_{1,2}(\bar m^2_{q,k},\bar m^2_{\sigma,k};\eta_{\phi,k})\\ &+(N_f^2-1)\bar h_k(\bar\kappa_k)^2\mathcal{M}_{1,2}(\bar m^2_{q,k},\bar m^2_{\pi,k};\eta_{\phi,k})].\end{aligned} \tag{B13}$$

The corresponding threshold functions can be in Eq. (C6).

Some of the flow equations in this work were derived with the aid of an extension of DoFun [51] which utilizes Form [52] and FormLink [53]. It was developed and first used by the authors of [3].

APPENDIX C: THRESHOLD FUNCTIONS

Here, we collect the threshold functions which enter the flow equations and encode the regulator and momentum dependence of the flows. Note that it is here that the substitution $\eta_{\phi,k} \to \eta_{\phi,k} - 2\tilde B_k$ has to be made according to (26).

Throughout this work, we use $4d$ regulator functions of the form

$$\begin{aligned}R^\phi_k(p^2) &= Z_{\phi,k}p^2r_B(p^2/k^2),\\ R^q_k(p^2) &= Z_{q,k}\gamma_\mu p_\mu r_F(p^2/k^2),\\ R^{A,\mu\nu}_k(p^2) &= Z_{A,k}p^2r_B(p^2/k^2)\Pi^\perp_{\mu\nu}(p),\end{aligned} \tag{C1}$$

with the transverse projector

$$\Pi^{\perp}_{\mu\nu}(p) = \delta_{\mu\nu} - \frac{p_\mu p_\nu}{p^2}. \tag{C2}$$

Note that in the approximation at hand the ghost regulator does not enter. The optimized regulator shape functions $r_{B/F}(x)$ are given by [29]

$$r_B(x) = \left(\frac{1}{x} - 1\right)\Theta(1-x),$$
$$r_F(x) = \left(\frac{1}{\sqrt{x}} - 1\right)\Theta(1-x). \tag{C3}$$

The threshold functions for the effective potential are

$$l^B_n(\bar{m}^2_B;\eta_B) = \frac{2(\delta_{n,0}+n)}{d}\left(1-\frac{\eta_B}{d+2}\right)(1+\bar{m}^2_B)^{-(n+1)},$$
$$l^F_n(\bar{m}^2_F;\eta_F) = \frac{2(\delta_{n,0}+n)}{d}\left(1-\frac{\eta_F}{d+1}\right)(1+\bar{m}^2_F)^{-(n+1)}, \tag{C4}$$

and that for the Yukawa coupling and the four-quark coupling are

$$L^{(FB)}_{1,1}(\bar{m}^2_F,\bar{m}^2_B;\eta_F,\eta_B) = \frac{2}{d}(1+\bar{m}^2_F)^{-1}(1+\bar{m}^2_B)^{-1}\left\{\left(1-\frac{\eta_F}{d+1}\right)(1+\bar{m}^2_F)^{-1} + \left(1-\frac{\eta_B}{d+2}\right)(1+\bar{m}^2_B)^{-1}\right\},$$
$$L^{(FB)}_{1,2}(\bar{m}^2_F;\eta_F,\eta_B) = \frac{2}{d}(1+\bar{m}^2_F)^{-2}\left\{2\left(1-\frac{2\eta_B}{d+2}\right) - \left(1-\frac{\eta_F}{d+1}\right) + 2(1+\bar{m}^2_F)^{-1}\left(1-\frac{\eta_F}{d+1}\right)\right\},$$
$$L^{(FB)}_{1,1,1}(\bar{m}^2_F,\bar{m}^2_{B1},\bar{m}^2_{B2};\eta_F,\eta_B) = \frac{2}{d}(1+\bar{m}^2_F)^{-2}(1+\bar{m}^2_{B1})^{-1}(1+\bar{m}^2_{B2})^{-1}\left\{[(1+\bar{m}^2_{B1})^{-1} + (1+\bar{m}^2_{B2})^{-1}]\right.$$
$$\left.\times\left(1-\frac{\eta_B}{d+2}\right) + [2(1+\bar{m}^2_F)^{-1}-1]\left(1-\frac{\eta_F}{d+1}\right)\right\}. \tag{C5}$$

For the anomalous dimensions, we have

$$\mathcal{M}_2(\bar{m}^2_F;\eta_F) = (1+\bar{m}^2_F)^{-4},$$
$$\mathcal{M}_{2,2}(\bar{m}^2_{B1},\bar{m}^2_{B2};\eta_B) = (1+\bar{m}^2_{B1})^{-2}(1+\bar{m}^2_{B2})^{-2}$$
$$\mathcal{M}_{1,2}(\bar{m}^2_F,\bar{m}^2_B;\eta_F,\eta_B) = \left(1-\frac{\eta_B}{d+1}\right)(1+\bar{m}^2_F)^{-1}(1+\bar{m}^2_B)^{-2}$$
$$\mathcal{M}_4(\bar{m}^2_F;\eta_F) = (1+\bar{m}^2_F)^{-4} + \frac{1-\eta_F}{d-2}(1+\bar{m}^2_F)^{-3} - \left(\frac{1}{4}+\frac{1-\eta_F}{2d-4}\right)(1+\bar{m}^2_F)^{-2}$$
$$\tilde{\mathcal{M}}_{1,1}(\bar{m}^2_F,\eta_F,\eta_B) = \frac{2}{d-1}(1+\bar{m}^2_F)^{-1}\left\{\frac{1}{2}\left(\frac{2\eta_F}{d}-1\right) + \left(1-\frac{\eta_B}{d+1}\right) + \left(1-\frac{2\eta_F}{d}\right)(1+\bar{m}^2_F)^{-1}\right\}. \tag{C6}$$

Finally, for the flow of $z_{\bar{q}Aq}$ we use

$$\mathcal{N}^{(m)}_{2,1}(\bar{m}^2_F,\bar{m}^2_B;\eta_F,\eta_B) = \frac{1}{d}\left(1-\frac{\eta_F}{d+1}\right)(1+\bar{m}^2_B)^{-1}\{2\bar{m}^2_F(1+\bar{m}^2_F)^{-3} + (1+\bar{m}^2_F)^{-2}\}$$
$$+\frac{1}{d}\left(1-\frac{\eta_B}{d+2}\right)(1+\bar{m}^2_B)^{-2}\{\bar{m}^2_F(1+\bar{m}^2_F)^{-2} + (1+\bar{m}^2_F)^{-1}\},$$
$$\mathcal{N}^{(g)}_{2,1}(\bar{m}^2_F;\eta_F,\eta_A) = \frac{1}{d}\left(1-\frac{\eta_F}{d+1}\right)\bar{m}^2_F(1+\bar{m}^2_F)^{-3} + \frac{1}{2d}\left(1-\frac{\eta_A}{d+2}\right)\bar{m}^2_F(1+\bar{m}^2_F)^{-2},$$
$$\mathcal{N}^{(g)}_{1,2}(\bar{m}^2_F;\eta_F,\eta_A) = \frac{1}{d+1}\left(1-\frac{\eta_F}{d+2}\right)\{2\bar{m}^2_F(1+\bar{m}^2_F)^{-2} - (1+\bar{m}^2_F)^{-1}\}$$
$$+\frac{4}{d+1}\left(1-\frac{\eta_A}{d+3}\right)(1+\bar{m}^2_F)^{-1}. \tag{C7}$$

APPENDIX D: INFRARED PARAMETER

In our study, we introduced an "infrared-strength" function $\varsigma_{a,b}(k)$ which we define as

$$\varsigma_{a,b}(k) = 1 + a\frac{(k/b)^{\delta}}{e^{(k/b)^{\delta}} - 1}, \tag{D1}$$

with $b > 0$ and $\delta > 1$. Note that the specific form of $\varsigma_{a,b}(k)$ is irrelevant for our result as long as it has the properties specified below. It defines a smooth step function centered around b which interpolates smoothly between

$$\varsigma_{a,b}(k \gg b) = 1 \quad \text{and} \quad \varsigma_{a,b}(k \ll b) = 1 + a. \tag{D2}$$

Thus, for $b = \mathcal{O}(1\ \text{GeV})$, $\varsigma_{a,b}(k)$ gives an IR enhancement, while it leaves the perturbative regime unaffected. We then modify the gauge couplings as

$$g_{s,k} \to \varsigma_{a,b}(k) g_{s,k}, \tag{D3}$$

where $g_{s,k} = g_{\bar{q}Aq,k}$, $g_{A^3,k}$, $g_{\bar{c}Ac,k}$. We choose the same parameters a and b for every gauge coupling. Accordingly, the flow equations of the gauge couplings then are

$$\partial_t g_{s,k} \to g_{s,k}\partial_t \varsigma_{a,b}(k) + \varsigma_{a,b}(k)\partial_t g_{s,k}. \tag{D4}$$

We have found that our results do not depend strongly on the precise value of b as long as it is $\mathcal{O}(1\ \text{GeV})$. To be specific, we choose $b = 1.3$ GeV for $\delta = 3$ in the following.

The parameter a is adjusted such that we get physical constituent quark masses in the infrared. Here, $a = 0.29$ yields $M_{q,0} = 299.5$ MeV, where $M_{q,k} = k\bar{m}_{q,k}$ is the renormalized quark mass.

Since the results in Ref. [3] demonstrate that the largest source for systematic errors of our truncation is rooted in the approximations that enter the flows of the gauge couplings, a procedure as discussed above is well justified.

[1] J. Braun, Eur. Phys. J. C **64**, 459 (2009).
[2] J. Braun, L. M. Haas, F. Marhauser, and J. M. Pawlowski, Phys. Rev. Lett. **106**, 022002 (2011).
[3] M. Mitter, J. M. Pawlowski, and N. Strodthoff, Phys. Rev. D **91**, 054035 (2015).
[4] J. Braun, L. Fister, T. Herbst, M. Mitter, J. M. Pawlowski, F. Rennecke, and N. Strodthoff (fQCD Collaboration).
[5] D. F. Litim and J. M. Pawlowski, arXiv:hep-th/9901063.
[6] J. Berges, N. Tetradis, and C. Wetterich, Phys. Rep. **363**, 223 (2002).
[7] J. M. Pawlowski, Ann. Phys. (Amsterdam) **322**, 2831 (2007).
[8] B.-J. Schaefer and J. Wambach, Phys. Part. Nucl. **39**, 1025 (2008).
[9] H. Gies, Lect. Notes Phys. **852**, 287 (2012).
[10] J. M. Pawlowski, AIP Conf. Proc. **1343**, 75 (2011).
[11] O. J. Rosten, Phys. Rep. **511**, 177 (2012).
[12] J. Braun, J. Phys. G **39**, 033001 (2012).
[13] L. von Smekal, Nucl. Phys. B, Proc. Suppl. **228**, 179 (2012).
[14] J. M. Pawlowski, Nucl. Phys. **A931**, 113 (2014).
[15] R. Alkofer and L. von Smekal, Phys. Rep. **353**, 281 (2001).
[16] C. D. Roberts and S. M. Schmidt, Prog. Part. Nucl. Phys. **45**, S1 (2000).
[17] C. S. Fischer, J. Phys. G **32**, R253 (2006).
[18] C. S. Fischer, A. Maas, and J. M. Pawlowski, Ann. Phys. (Amsterdam) **324**, 2408 (2009).
[19] D. Binosi and J. Papavassiliou, Phys. Rep. **479**, 1 (2009).
[20] A. Maas, Phys. Rep. **524**, 203 (2013).
[21] P. Boucaud, J. Leroy, A. L. Yaouanc, J. Micheli, O. Pene *et al.*, Few-Body Syst. **53**, 387 (2012).
[22] H. Gies and C. Wetterich, Phys. Rev. D **65**, 065001 (2002).
[23] H. Gies and C. Wetterich, Phys. Rev. D **69**, 025001 (2004).
[24] S. Floerchinger and C. Wetterich, Phys. Lett. B **680**, 371 (2009).
[25] L. Fister and J. M. Pawlowski, arXiv:1112.5440.
[26] L. Fister and J. M. Pawlowski (to be published).
[27] J. M. Pawlowski and F. Rennecke, Phys. Rev. D **90**, 076002 (2014).
[28] C. Wetterich, Phys. Lett. B **301**, 90 (1993).
[29] D. F. Litim, Phys. Lett. B **486**, 92 (2000).
[30] U. Ellwanger, Phys. Lett. B **335**, 364 (1994).
[31] M. D'Attanasio and T. R. Morris, Phys. Lett. B **378**, 213 (1996).
[32] Y. Igarashi, K. Itoh, and H. So, Prog. Theor. Phys. **106**, 149 (2001).
[33] C. S. Fischer, J. Luecker, and J. A. Mueller, Phys. Lett. B **702**, 438 (2011).
[34] C. S. Fischer and J. Luecker, Phys. Lett. B **718**, 1036 (2013).
[35] C. S. Fischer, L. Fister, J. Luecker, and J. M. Pawlowski, Phys. Lett. B **732**, 273 (2014).
[36] C. S. Fischer, J. Luecker, and J. M. Pawlowski, Phys. Rev. D **91**, 014024 (2015).
[37] L. Fister, Ph.D. thesis, Heidelberg University, 2012.
[38] M. Q. Huber and L. von Smekal, J. High Energy Phys. 04 (2013) 149.
[39] M. Pelaez, M. Tissier, and N. Wschebor, Phys. Rev. D **88**, 125003 (2013).
[40] G. Eichmann, R. Williams, R. Alkofer, and M. Vujinovic, Phys. Rev. D **89**, 105014 (2014).
[41] A. Blum, M. Q. Huber, M. Mitter, and L. von Smekal, Phys. Rev. D **89**, 061703 (2014).

[42] D. Binosi, D. Ibanez, and J. Papavassiliou, J. High Energy Phys. 09 (2014) 059.
[43] J. Gracey, Phys. Rev. D **90**, 025014 (2014).
[44] A. K. Cyrol, M. Q. Huber, and L. von Smekal, Eur. Phys. J. C **75**, 102 (2015).
[45] M. Hopfer, A. Windisch, and R. Alkofer, *Proc. Sci.*, ConfinementX2012 (2012) 073 [arXiv:1301.3672].
[46] R. Williams, Eur. Phys. J. A **51**, 57 (2015).
[47] A. Aguilar, D. Binosi, D. Ibanez, and J. Papavassiliou, Phys. Rev. D **90**, 065027 (2014).
[48] A. J. Helmboldt, J. M. Pawlowski, and N. Strodthoff, Phys. Rev. D **91**, 054010 (2015).
[49] N. Strodthoff, B.-J. Schaefer, and L. von Smekal, Phys. Rev. D **85**, 074007 (2012).
[50] T. K. Herbst, M. Mitter, J. M. Pawlowski, B.-J. Schaefer, and R. Stiele, Phys. Lett. B **731**, 248 (2014).
[51] M. Q. Huber and J. Braun, Comput. Phys. Commun. **183**, 1290 (2012).
[52] J. A. M. Vermaseren, arXiv:math-ph/0010025.
[53] F. Feng and R. Mertig, arXiv:1212.3522.